Fig. 3 (Contd.)

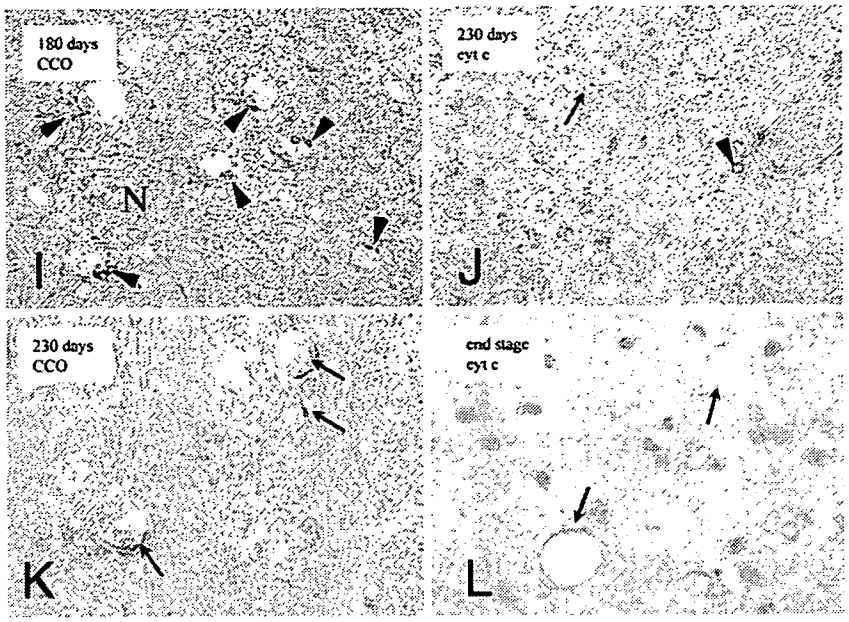

seen only rarely (Fig. 3j, l), and some large vacuoles were observed scattered throughout the neuropil. The CCO-positive structures lying interior to the vacuole rim became atrophic (Fig. 3k), especially in moribund mice. Cyt *c*-positive vacuoles were never seen in the soma of neurons from G1L mice.

Immunohistochemical analyses of vacuoles in the lumbar segment of G1H mice

In symptomatic G1H mice (100 and 115 days), prominent vacuole formation was observed (Fig. 4b, c, e, f). The vacuolar rims were cyt-*c*-positive and there were

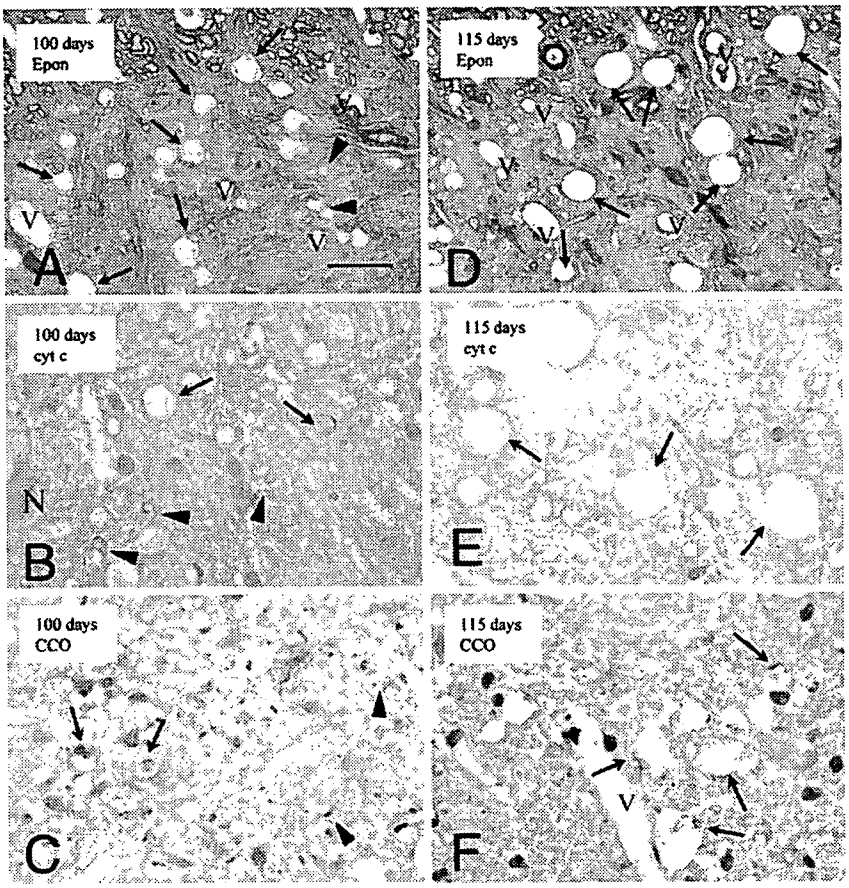

Fig. 4 More prominent vacuole formation with similar immunostaining patterns for cyt *c* and CCO in the anterior horn of G1H mice (**a–c**; 100 days, **b–f**; 115 days, **a**, **d**; Epon sections, toluidine blue, **b**, **e**; cyt *c*, **c**, **f**; CCO). **a** Abundant small (< 5 μm, *arrow heads*) or large (> 5 μm, *arrows*) vacuoles are present in neurites. **b** Cyt-*c*-positive staining in the rim of small (*arrow heads*) and large (*arrows*) vacuoles. The immunoreactivity of the large vacuoles (*arrows*) is reduced, as in G1L mice. **c** CCO-positive structures are evident in small (*arrow heads*) or large vacuoles (*arrows*). **d** The number of vacuoles is reduced. Larger vacuoles than those in **a** are frequently evident. **e** Large vacuoles about 15–20 μm in diameter (*arrows*) are observed more frequently than in the G1L lumbar segment. **f** Somewhat atrophic CCO-positive structures (*arrows*) lying interior to the rim of large vacuoles. *N* neurons; *V* vessels. Scale bar, **a** (also for **b–f**) 20 μm

CCO-positive structures lying interior to them, as observed in G1L mice. Cyt *c* immunoreactivity was reduced in the large vacuoles (Fig. 4b, e). The structures lying interior to the vacuolar rim, evident at 100 days (Fig. 4c), became rather atrophic by 115 days (Fig. 4f). At 100 days, the ratio of the number of large vacuoles (> 5 μm) to the total number of vacuoles was more than 50% (Fig. 4b); this figure had reached almost 90–100% by 115 days (Fig. 4e). The vacuoles in G1H mice tended to be larger than those in G1L mice.

Quantitative analysis of the vacuoles, LBHIs and motor neurons in the lumbar segment of G1L and G1H mice

Figure 5 shows the number of small (< 5 μm) and large (> 5 μm) vacuoles, and LBHIs and motor neurons (> 25 μm) in the lumbar segment during the clinical course of the disease in G1L mice. Numerous small vacuoles were already evident at 90 days, and their number decreased as the disease progressed (Fig. 5a, Table 1, $P < 0.05$). The number of large vacuoles, which appeared at around 140 days, were increased significantly by 180 days but then decreased significantly by 230 days (Fig. 5a, Table 1, $P < 0.05$). The ratio of the number of large vacuoles to the total number of vacuoles was 10–20% at 140 and 180 days, and ~50% in moribund mice (Fig. 5a). In G1H mice, the total number of vacuoles showed a tendency to decrease, but not to a significant degree (Table 1, $P = 0.1266$). The number of neurons declined significantly after 180 days in G1L mice, and after 66 days in G1H mice (Table 1, $P < 0.05$). LBHIs were restricted to the anterior horn at 180 and 100 days in G1L and G1H mice, respectively, becoming more widespread at the later stages. The number of LBHIs increased significantly in G1L or G1H mice as the disease progressed (Fig. 5b, Table 1, $P < 0.05$). Most of the LBHIs were intra-neuritic.

Correlation between the numbers of vacuoles and LBHIs in symptomatic G1L and G1H mice

Figure 6 shows the correlation between the numbers of vacuoles and LBHIs observed in symptomatic G1L (230 days and in the moribund state) and G1H (100 and 115 days) mice. The number of vacuoles in G1H mice was greater than in G1L mice. Regression analysis revealed a statistically significant inverse correlation between the numbers of vacuoles and LBHIs in both G1L ($r = -0.91$, $P < 0.01$) and G1H ($r = -0.93$, $P < 0.01$) mice.

Quantitative analysis of LBHIs in the nVII and the differential localization of LBHIs and vacuoles

HE staining revealed atrophic motor neurons with prominent vacuole formation in the nVII of moribund G1L mice. Most of the vacuoles in the nVII (Fig. 7b)

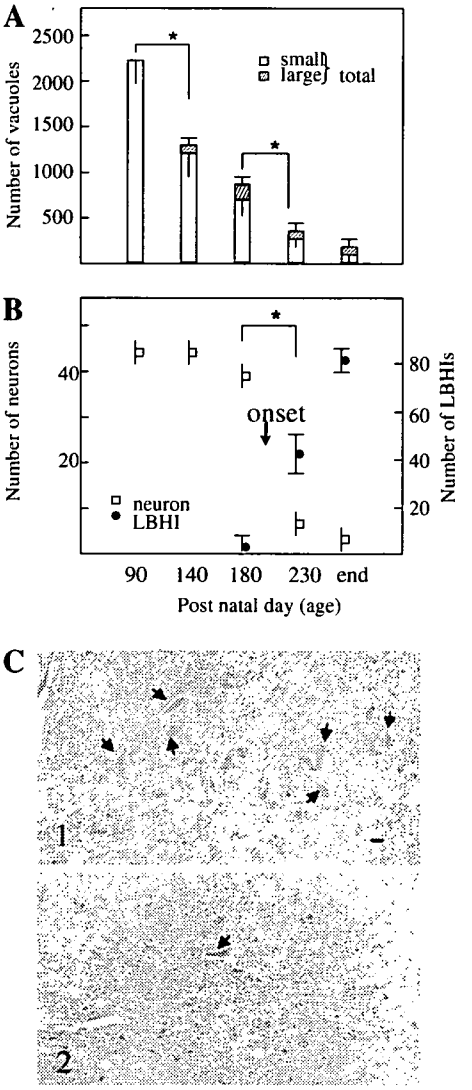

Fig. 5 Time course of changes in the number of vacuoles (**a**), LBHIs and motor neurons (**b**) in the anterior horn of G1L mice. **a** Numerous small vacuoles are evident at 90 days. The number of small vacuoles decreases significantly with disease progression (*$P < 0.05$). The large vacuoles are present from 140 days, and their number then increases significantly by 180 days, followed by a significant decrease by 230 days. **b** The number of neurons (> 25 μm) declines significantly after 180 days (*$P < 0.05$) and, conversely, the number of LBHIs increases significantly after 180 days (*$P < 0.05$). Data are presented as mean ± SEM ($n = 3$ for each group). **c** Representative hematoxylin and eosin (HE) staining of the anterior horn in control (**1**) and G1L mice at the end stage (**2**). The number of neurons (> 25 μm, *arrows*) is reduced in (**2**). Scale bar **c** 25 μm

were larger than those observed in the lumbar segment. The number of motor neurons in the nVII was significantly reduced (Table 2, $P < 0.05$), and LBHIs were found only rarely in the vacuole-rich area (= intra-nVII). In marked contrast, LBHIs were found frequently in the border zone (see Materials and methods), but there were very few vacuoles (Fig. 7c). Most of the vacuoles were located in the neuropil, and not in the soma of neurons (Fig. 7d). Most of the LBHIs were also

Table 1 Number of anterior horn cells, vacuoles and LBHIs in the lumbar segments of G1L and G1H mice (values are given as mean ± SEM)

	G1L						G1H		
	90 days	140 days	180 days	230 days	259 ± 6 days	Non-transgenic (260 ± 6 days)	66 days	100 days	115 days
Anterior horn cells	43 ± 1	43 ± 2	39 ± 2	8 ± 3[b]	4 ± 1[b]	41 ± 1	41 ± 2	31 ± 3[c]	14 ± 3[d]
Vacuoles (total)	2,243 ± 151	1,307 ± 188[a]	842 ± 139[a]	314 ± 42[b]	198 ± 115[b]	0	ND	1,832 ± 259	1,078 ± 201
LBHIs	0	0	4 ± 3	44 ± 18[b]	83 ± 6[b]	0	0	11 ± 3	30 ± 6[d]

G1L Mutant SOD1 (G93A) low-copy mouse; *G1H* mutant SOD1 (G93A) high-copy mouse; *SEM* standard error of the mean; *LBHI* Lewy-body-like hyaline inclusion; *ND* not determined
[a] $P < 0.05$ compared with G1L mice at 90 days; [b] $P < 0.05$ compared with G1L mice at 180 days; [c] $P < 0.05$ compared with G1H mice at 66 days; [d] $P < 0.05$ compared with G1H mice at 100 days

intra-neuritic. The LBHIs in the border zone were larger than those in the vacuole-rich area (=intra-nVII). Quantitative analysis of data from the three subregions of the pons demonstrated a preferential localization of LBHIs to the border zone, the area surrounding the nVII (Table 2, $P < 0.01$).

Immunohistochemical analysis of vacuoles in the facial nucleus of G1L mice

Immunohistochemical analysis of vacuoles in the facial nucleus (nVII) showed that abundant tiny cyt-*c*-positive vacuoles appeared at the edge of the nVII at an early stage (Fig. 8a), similar to those in the lumbar segments. As the disease progressed, the vacuoles became larger (Fig. 8b–f) and were distributed throughout the nVII. Thereafter, although their number decreased progressively, a considerable amount of large vacuoles remained in the nVII even at the end stage (Figs. 7b, 8f). The immunoreactivity for cyt-*c* was weaker in the larger vacuoles than in the tiny vacuoles (Fig. 8b). Immunohistochemical staining for mutant SOD1 showed that the rim of the vacuoles was stained at an early stage (Fig. 8c, d). The SOD1 immunoreactivity of the rim increased at 140 days (Fig. 8d). By 180 days, not only the rim, but also the core of the vacuoles became SOD1-positive (Fig. 8e). At the end stage, the SOD1-positive structures inside the vacuoles decreased. Most of the vacuoles, except for those present in axons, showed weak immunoreactivity for SOD1 in their rim. Vacuoles that were almost SOD1-negative were frequently observed (Fig. 8f).

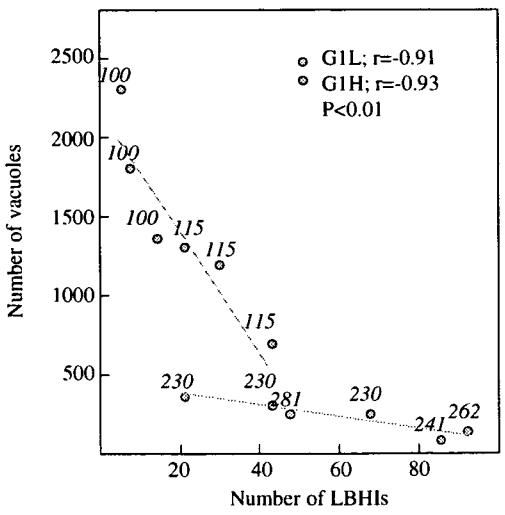

Fig. 6 Inverse correlation between the numbers of mitochondria-derived vacuoles and LBHIs. A statistically significant inverse correlation was observed between the numbers of LBHIs and vacuoles in both G1L (*green*) and G1H (*orange*) mice. Numbers shown in *italics* represent the age of the G93A mice at perfusion

Discussion

In the G93A mouse, the most commonly studied model of ALS, the characteristic neuropathological features are LBHIs and vacuoles [6, 7]. Although scarcely found in FALS patients associated with SOD1 gene mutation [41], it has been considered important to investigate vacuoles [18, 19, 28, 42, 43] because the model mice overexpressing the mutant SOD1 protein could provide clues for understanding the characteristics of mutant SOD1. Also, since evaluation of LBHIs, which are the hallmarks of FALS linked with SOD1 gene mutation, is indispensable for pathological analysis, it is necessary to clarify the factors that can influence their formation.

In control mice, the cytoplasm of the motor neurons showed granular staining with antibodies against subunit I of CCO, a component of the mitochondrion-specific enzyme that is localized in the inner membrane [50], and against cyt *c*, a mediator of CCO that is localized in the intermembrane space [38]. The staining with these antibodies in the motor neurons of control mice corresponds to the localization of mitochondria [11, 19]. In G93A mice, the rims of vacuoles were cyt-*c*-positive and CCO-negative, and the structures lying interior to the vacuolar rim were CCO-positive and cyt-*c*-negative. The latter structures are probably non-functional mitochondrial membrane remnants [14, 28, 43]. Since cyt *c* is released into the cytosol from the permeability transition pores of injured mitochondria [11, 27, 29, 45, 47, 57, 58], the presence of a cyt-*c*-positive

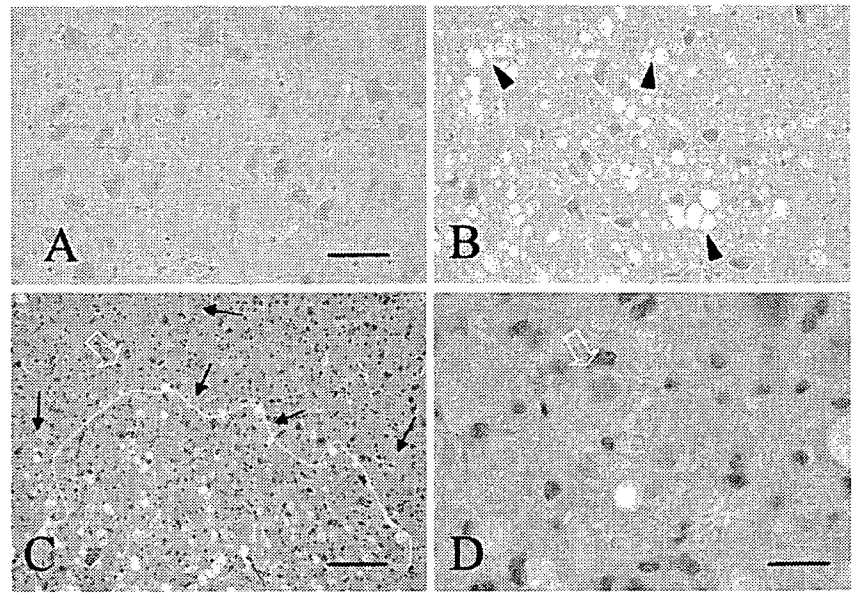

Fig. 7 Representative hematoxylin and eosin staining in the nVII of control (**a**; 261 days) and G1L (**b–d**; end stage) mice. **a**, **b** The number of motor neurons in the G1L nVII is reduced, and all of the residual neurons are atrophic in G1L mice as compared with the controls. Note the prominent vacuolization (*arrow heads*) and lack of LBHIs inside the G1L nVII. **c** Many LBHIs are present (*arrows*, *white arrow*) in the area surrounding the nVII. The *yellow line* delineates the vacuole-rich area (= intra-nVII). **d** A large LBHI (*white arrow*), more than 10 μm in diameter, is located in a neurite, and not in the soma. Scale bar **a** (also for **b**) 50 μm, **c** 100 μm, and **d** 20 μm

rim might imply that cyt *c* is released from the intermembrane space of injured mitochondria into vacuoles to accumulate along the vacuolar rim. Since both small (< 5 μm) and large (> 5 μm) vacuoles in the neuropil exhibited the same immunostaining patterns for cyt *c* and CCO, and since small vacuoles did not appear to fuse to form large ones, it is thought that the small vacuoles grow to become the large vacuoles [14].

According to a previous report, the appearance of vacuoles in the lumbar segments might be related to the onset, rather than progression of the disease, since the number of vacuoles was found to be maximal at disease onset, and declined thereafter [28]. Using antibodies against mitochondrial components, we have shown here that numerous tiny vacuoles, which are distinguishable from cyt-*c*-negative capillary blood vessels, appear in the neuropil approximately 3.5 months before disease onset [14, 19]. In G1L mice, the number of vacuoles in both the lumbar segment and brainstem decreased progressively thereafter, irrespective of disease onset. In contrast with the findings of the previous study [28], therefore, we have found that the presence of these vacuoles appears to be unrelated to disease onset. Although the number of large vacuoles (> 5 μm) increased until disease onset and decreased thereafter, they appeared to be unrelated to disease onset because the degree of neuron loss in the nVII, exhibiting prominent large vacuoles, was much less marked than in the lumbar segment. If the presence of large vacuoles had been related to disease onset, which is determined by neuron loss, then the degree of neuronal loss in the nVII would have been more severe.

In the lumbar segment, intra-neuritic LBHIs appeared just before disease onset and increased rapidly [55] with the progressive reduction in the number of vacuoles in neurites [28, 42, 43]. Although the number of vacuoles was greater in G1H mice than in G1L mice, there was a statistically significant inverse correlation between the number of vacuoles and LBHIs in symptomatic G1L and G1H mice. In the G1L brainstem with prominent vacuole formation, the number of motor neurons was significantly reduced, in agreement with previous reports [13, 35], but only a few LBHIs were found even at the end stage. A notable observation was the presence of many intra-neuritic LBHIs in the border zone where there were few vacuoles. As LBHI formation is known to occur in affected neurons [15, 44, 54], the LBHIs around the nVII would be contained within the neurites of motor neurons in that area. Therefore, there was an inverse correlation between these two neuro-

Table 2 Number of motor neurons and density of LBHIs in the pons divided into three subregions; vacuole-rich area (= intra-nVII), the border zone and vacuole-poor area (values are given as mean ± SEM)

	Age (days)	Number of motor neurons	Density of LBHIs		
			Vacuole-rich area	Border zone	Vacuole-poor area
G1L	258 ± 7	163 ± 8[a]	1.6 ± 0.5[b]	22 ± 8	1.8 ± 0.7[b]
Non-transgenic	264 ± 7	242 ± 3	0	0	0

nVII facial nucleus; *G1L* mutant SOD1 (G93A) low-copy mouse; *SEM* standard error of the mean; *LBHI* Lewy-body-like hyaline inclusion

The density of LBHIs is the number of LBHIs per 1 mm^2 area

[a] $P < 0.05$ compared with non-transgenic mice; [b] $P < 0.01$ compared with border zone

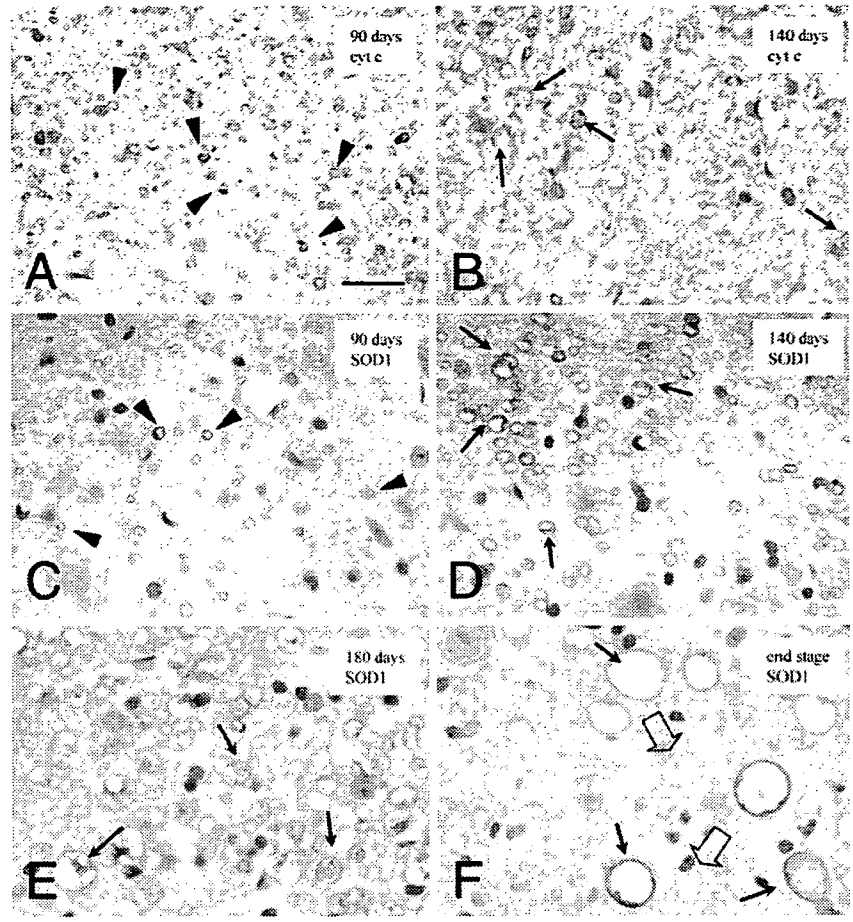

Fig. 8 Immunohistochemical analysis of vacuoles in the nVII of G1L mice (**a**, **c**; 90 days, **b**, **d**; 140 days, **e**; 180 days, **f**; end stage, **a**, **b**; cyt-*c*, **c**–**f**; SOD1). **a** Many tiny cyt-*c*-positive vacuoles (*arrow heads*) are evident. **b** Larger vacuoles (*arrows*) appear, showing lower immunoreactivity than in **a**. **c** Tiny vacuoles (*arrow heads*) are SOD1-positive. **d** SOD1 immunoreactivity becomes stronger at the rim of larger vacuoles (*arrows*) than that of tiny vacuoles observed in **c**. **e** SOD1-positivity is evident not only at the rim, but also the core of the vacuoles (*arrows*). The immunoreactivity has become stronger than that in **d**. **f** Only a few large vacuoles (*arrows*, *clear arrows*) remain. The SOD1 immunoreactivity of vacuoles has become weaker than that in **e**. Some of the vacuoles (*clear arrows*) are almost immunonegative. Scale bar **a** (also for **b**–**f**) 20 μm

pathological changes in both the lumbar segment and the nVII.

Immunohistochemistry using anti-SOD1 antibody revealed that mutant SOD1 accumulated in the rim of tiny vacuoles at an early stage, and was increased in both the rim and the core of the vacuoles [19, 43] until onset. After onset, the intensity of SOD1 immunostaining decreased in both the rim and the core, and SOD1-negative large vacuoles were frequently observed. Since the amount of mutant SOD1 protein increases with age [19, 51], the increased SOD1 immunoreactivity in vacuoles would suggest that more mutant SOD1 was retained in them before onset. The fact that the SOD1 immunoreactivity in vacuoles decreased after onset suggests that vacuoles would not be able to sequester mutant SOD1, despite its higher level of expression in neurons. It is possible that only well-functioning vacuoles at the early stage might be able to retain mutant SOD1. Since mutant SOD1 does not disappear, even when it leaks from vacuoles after onset, it would still remain in the cell [52]. Mutant SOD1 that increased outside vacuoles but remained within the cell would be related to the formation of LBHIs, followed by aggregation of mutant SOD1 in the cell.

In a study using electron and immunofluorescence microscopy, Higgins et al. have reported that the vacuoles originate through expansion of the mitochondrial intermembrane space and extension of the outer mitochondrial membrane and lack lysosomal signals [14]. This suggests that the vacuoles would be produced by a nonautophagic, but still uncharacterized and unique mechanism. In this study, we found a negative correlation between the mitochondria-derived vacuoles and LBHIs, although this does not necessarily mean that the former prevents the latter. However, considering the results of SOD1 immunostaining, it is not unlikely that the mitochondria-derived vacuoles might prevent the formation of LBHIs by sequestering mutated SOD1 from the cytoplasm.

Acknowledgment This study was supported in part by a Health and Labour Sciences Research Grant, Research on Measures for Incurable Disease, Ministry on Health, Labour and Welfare of Japan.

References

1. Barneoud P, Lolivier J, Sanger DJ, Scatton B, Moser P (1997) Quantitative motor assessment in FALS mice: a longitudinal study. Neuroreport 8:2861–2865
2. Bruening W, Roy J, Giasson B, Figlewicz DA, Mushynski WE, Durham HD (1999) Up-regulation of protein chaperones preserves viability of cells expressing toxic Cu/Zn-superoxide dismutase mutants associated with amyotrophic lateral sclerosis. J Neurochem 72:693–699

3. Brujin LI, Becher MW, Lee MK, Anderson KL, Jenkins NA, Copeland NG, Sisodia SS, Rothstein JD, Borchelt DR, Price DL, Cleveland DW (1997) ALS-linked SOD1 mutant G85R mediates damage to astrocytes and promotes rapidly progressive disease with SOD1-containing inclusions. Neuron 18:327–338
4. Brujin LI, Houseweart MK, Kato S, Anderson KL, Anderson SD, Ohama E, Reaume AG, Scott RW, Cleveland DW (1998) Aggregation and motor neuron toxicity of an ALS-linked SOD1 mutant independent from wild-type SOD1. Science 281:1851–1854
5. Cleveland DW, Liu J (2000) Oxidation versus aggregation—how do SOD1 mutants cause ALS? Nat Med 6(12):1320–1321
6. Dal Canto MC, Gurney ME (1994) Development of central nervous system pathology in a murine transgenic model of human amyotrophic lateral sclerosis. Am J Pathol 145:1271–1279
7. Dal Canto MC, Gurney ME (1997) A low expressor line of transgenic mice carrying a mutant human Cu, Zn superoxide dismutase (SOD1) gene develops pathological changes that most closely resemble those in human amyotrophic lateral sclerosis. Acta Neuropathol 93:537–550
8. Deng H-X, Hentati A, tainer JA, Iqbal Z, Cayabyab A, Hung WY, Getsoff ED, Hu P, Herzfeldt B, Roos RP, Warner C, Deng G, Soriano E, Smyth C, Parge HE, Ahmed A, Roses AD, Hallwell RA, Pericak-Vance MA, Siddique T (1993) Amyotrophic lateral sclerosis and structural defects in Cu/Zn superoxide dismutase. Science 261:1047–1051
9. Durham HD, Roy J, Dong L, Figlewicz DA (1997) Aggregation of mutant Cu/Zn superoxide dismutase proteins in a culture model of ALS. J Neuropathol Exp Neurol 56(5):523–530
10. Fischer LR, Culver DG, Tennant P, Davis AA, Wang M, Castellano-Sanchez A, Khan J, Polak MA, Glass JD (2004) Amyotrophic lateral sclerosis is a distal axonopathy: evidence in mice and man. Exp Neurol 185:232–240
11. Guegan C, Vila M, Rosoklija G, Hays AP, Przedborski S (2001) Recruitment of the mitochondrial-dependent apoptotic pathway in amyotrophic lateral sclerosis. J Neurosci 21:6569–6576
12. Gurney ME, Pu H, Chiu AY, Dal Canto MC, Polchow CY, Alexander DD, Caliendo J, Hentati A, Kwon YW, Deng HX, Chen W, Zhai P, Sufit RL, Siddique T (1994) Motor neuron degeneration in mice that express a human Cu, Zn superoxide dismutase mutation. Science 264:1772–1775
13. Haenggeli C, Kato AC (2002) Differential vulnerability of cranial motoneurons in mouse models with motor neuron degeneration. Neurosci Lett 335:39–43
14. Higgins CMJ, Jung C, Xu Z (2003) ALS-associated mutant $SOD1^{G93A}$ causes mitochondrial vacuolation by expansion of the intermembrane space and by involvement of SOD1 aggregation and peroxisomes. BMC Neurosci 4:16
15. Hirano A, Kurland LT, Sayre GP (1967) Familial amyotrophic lateral sclerosis. A subgroup characterized by posterior and spinocerebellar tract involvement and hyaline inclusions in the anterior horn cells. Arch Neurol 16:232–243
16. Howland DS, Jiu J, She Y, Goad B, Maragakis NJ, Kim B, Erickson J, Kulik J, DeVito L, Psaltis G, DeGennaro LJ, Cleveland DW, Rothstein JD (2002) Focal loss of the glutamate transporter EAAT2 in a transgenic rat model of SOD1 mutant-mediated amyotrophic lateral sclerosis (ALS). Proc Natl Acad Sci USA 99:1604–1609
17. Inoue K, Fujimura H, Ogawa Y, Satoh T, Shimada K, Sakoda S (2002) Familial amyotrophic lateral sclerosis with a point mutation (G37R) of the superoxide dismutase 1 gene: a clinicopathological study. Amyotroph Lateral Scler Other Motor Neuron Disord 3:244–247
18. Jaarsma D, Haasdijk ED, Grashorn JAC, Hawkins R, Dujin WV, Verspaget HW, London J, Holstege JC (2000) Human Cu/Zn superoxide dismutase (SOD1) overexpression in mice causes mitochondrial vacuolization, axonal degeneration, and premature motoneuron death and accelerates motoneuron disease in mice expressing a familial amyotrophic lateral sclerosis mutant SOD1. Neurobiol Dis 7:623–643
19. Jaarsma D, Rognoni F, Duijn WV, Verspaget HW, Haasdijk ED, Holstege JC (2001) CuZn superoxide dismutase (SOD1) accumulates in vacuolated mitochondria in transgenic mice expressing amyotrophic lateral sclerosis-linked SOD1 mutations. Acta Neuropathol 102:293–305
20. Johnston JA, Ward CL, Kopito RR (1998) Aggresomes: a cellular response to misfolded proteins. J Cell Biol 143:1883–1898
21. Johnston JA, Dalton MJ, Gurney ME, Kopito RR (2000) Formation of high molecular weight complexes of mutant Cu,Zn-superoxide dismutase in a mouse model for familial amyotrophic lateral sclerosis. Proc Natl Acad Sci USA 97:12571–12576
22. Kato S, Takikawa M, Nakashima K, Hirano A, Cleveland DW, Kusaka H, Shibata N, Kato M, Nakano I, Ohama E (2000) New consensus research on neuropathological aspects of familial amyotrophic lateral sclerosis with superoxide dismutase 1 (SOD1) gene mutations: inclusions containing SOD1 in neurons and astrocytes. Amyotroph Lateral Scler Other Motor Neuron Disord 1:163–184
23. Kato S, Horiuchi S, Liu J, Cleveland DW, Shibara N, Nakashima K, Nagai R, Hirano A, Takikawa M, Kato M, Nakano I, Ohama E (2000) Advanced glycation endproduct-modified superoxide dismutase-1 (SOD1)-positive inclusions are common to familial amyotrophic lateral sclerosis patients with SOD1 gene mutations and transgenic mice expressing human SOD1 with a G85R mutation. Acta Neuropathol 100:490–505
24. Kato S, Sumi-Akamaru H, Fujimura H, Sakoda S, Kato M, Hirano A, Takikawa M, Ohama E (2001) Copper chaperone for superoxide dismutase co-aggregates with superoxide dismutase 1 (SOD1) in neuronal Lewy body-like hyaline inclusions: an immunohistochemical study on familial amyotrophic lateral sclerosis with SOD1 gene mutation. Acta Neuropathol 102:233–238
25. Kato S, Saeki Y, Aoki M, Nagai M, Ishizaki A, Itoyama Y, Kato M, Asayama K, Awaya A, Hirano A, Ohama E (2004) Histological evidence of redox system breakdown caused by superoxide dismutase 1 (SOD1) aggregation is common to SOD1-mutated motor neurons in humans and animal models. Acta Neuropathol 107:149–158
26. Klivenyi P, Ferrante RJ, Mathews RT, Bogdanov MB, Klein AM, Andreassen OA, Mueller G, Wermer M, Kaddurah-Daouk R, Flint Beal M (1999) Neuroprotective effects of creatine in a transgenic animal model of amyotrophic lateral sclerosis. Nat Med 5:347–351
27. Kluck RM, Bossy-Wetzel E, Green DR, Newmeyer DD (1997) The release of cytochrome *c* from mitochondria: a primary site for Bcl-2 regulation of apoptosis. Science 275:1132–1136
28. Kong J, Xu Z (1998) Massive mitochondrial degeneration in motor neurons triggers the onset of amyotrophic lateral sclerosis in mice expressing a mutant SOD1. J Neurosci 18(9):3241–3250
29. Liu X, Kim CN, Yang J, Jemmerson R, Wang X (1996) Induction of apoptotic program in cell-free extracts: requirement for dATP and cytochrome *c*. Cell 86:147–157
30. McHanwell S, Biscoe TJ (1981) The sizes of motoneurons supplying hindlimb muscles in the mouse. Proc R Soc Lond 213:201–216
31. Mohajeri MH, Figlewicz DA, Bohn MC (1998) Selective loss of α motoneurons innervating the medial gastrocnemius muscle in a mouse model of amyotrophic lateral sclerosis. Exp Neurol 150:329–336
32. Nagai M, Aoki M, Miyoshi I, Kato M, Pasinelli P, Kasai N, Brown RH Jr, Itoyama Y (2001) Rats expressing human cytosolic copper-zinc superoxide dismutase transgenes with amyotrophic lateral sclerosis: associated mutations develop motor neuron disease. J Neurosci 21(23):9246–9254
33. Nagano S, Ogawa Y, Yanagihara T, Sakoda S (1999) Benefit of a combined treatment with trientine and ascorbate in familial amyotrophic lateral scledosis model mice. Neurosci lett 265:159–162

34. Nagano S, Satoh M, Sumi H, Fujimura H, Tohyama C, Yanagihara T, Sakoda S (2001) Reduction of metallothioneins promotes the disease expression of familial amyotrophic lateral sclerosis mice in a dose-dependent manner. Eur J Neurosci 13:1363–1370
35. Nimchinsky EA, Young WG, Yeung G, Shah RA, Gordon JW, Bloom FE, Morrison JH, Hof PR (2000) Differential vulnerability of oculomotor, facial, and hypoglossal nuclei in G86R superoxide dismutase transgenic mice. J Comp Neurol 416:112–125
36. Olanow CW, Perl DP, DeMartino GN, McNaught KSP (2004) Lewy-body formation is an aggresome-related process: a hypothesis. Lancet Neurol 3:496–503
37. Paxinos G, Franklin KBJ (2001) The mouse brain in stereotaxic coordinates second edition. Academic Press, Figs 79–85
38. Reed JC (1997) Cytochrome *c*: can't live with it-can't live without it. Cell 91:559–562
39. Ripps ME, Huntley GW, Hoff PR, Morrison JH, Gordon JW (1995) Transgenic mice expressing an altered murine superoxide dismutase gene provide an animal model of amyotrophic lateral sclerosis. Proc Natl Acad Sci USA 92:689–693
40. Rosen DR, Siddique T, Patterson D, Figlewicz DA, Sapp P, Hentati A, Donaldson D, Goto J, O'Regan JP, Deng H-X, Rahmani Z, Krizus A, Mckenna-Yasek D, Cayabyab A, Gaston SM, Berger R, Tanzi RE, Halperin JJ, Herzfeldt B, Van den Bergh R, Hung W-Y, Bird T, Deng G, Mulder DW, Smyth C, Laing NG, Soriano E, Pricak-Vance MA, Haines J, Rouleau GA, Gusella JS, Horritz HR, Brown RH (1993) Mutations in Cu/Zn superoxide dismutase gene are associated with familial amyotrophic lateral sclerosis. Nature 362:59–62
41. Sasaki S, Ohsawa Y, Yamane K, Sakuma H, Shibata H, Nakano R, Kikugawa K, Mizutani T, Tsuji S, Iwata M (1998) Familial amyotrophic lateral sclerosis with widespread vacuolation and hyaline inclusions. Neurology 51:871–873
42. Sasaki S, Warita H, Abe K, Iwata M (2004) Slow component of axonal transport is impaired in the proximal axon of transgenic mice with G93A mutant SOD1 gene. Acta Neuropathol 107:452–460
43. Sasaki S, Warita H, Murakami T, Abe K, Iwata M (2004) Ultrastructural study of mitochondria in the spinal cord of transgenic mice with a G93A mutant SOD1 gene. Acta Neuropathol 107:461–474
44. Shibata N, Hirano A, Kobayashi M, Siddique T, Deng HX, Hung WY, Kato T, Asayama K (1996) Intense superoxide dismutase-1 immunoreactivity in intracytoplasmic hyaline inclusions of familial amyotrophic lateral sclerosis with posterior column involvement. J Neuropathol Exp Neurol 55:481–490
45. Shimizu S, Narita M, Tsujimoto Y (1999) Bcl-2 family proteins regulate the release of apoptogenic cytochrome *c* by the mitochondrial channel VDAC. Nature 399:486–487
46. Stathopulos PB, Rumfeldt JAO, Scholzs GA, Irani RA, Frey HE, Hallewell RA, Lepock JR, Meiering EM (2003) Cu/Zn superoxide dismutase mutants associated with amyotrophic lateral sclerosis show enhanced formation of aggregates in vitro. Proc Natl Acad Sci USA 100(12):7021–2026
47. Steiber A, Gonatas JO, Gonatas NK (2000) Aggregation of ubiquitin and a mutant ALS-linked SOD1 protein correlate with disease progression and fragmentation of the Golgi apparatus. J Neurol Sci 173:53–62
48. Stephens B, Navarrete R, Guiloff RJ (2001) Ubiquitin immunoreactivity in presumed spinal interneurons in motor neurone disease. Neuropathol Appl Neurobiol 27:352–361
49. Sugai F, Yamamoto Y, Miyaguchi K, Zhou Z, Sumi H, Hamasaki T, Goto M, Sakoda S (2004) Benefit of valproic in suppressing disease progression of ALS model mice. Eur J Neurosci 20:3179–3183
50. Tsukihara T, Aoyama H, Yamashita E, Tomizaki T, Yamaguchi H, Shinzawa-Itoh K, Nakashima R, Yaono R, Yoshikawa S (1996) The whole structure of the 13-subunit oxidized cytochrome *c* oxidase at 2.8A. Science 272:1136–1144
51. Turner BJ, Lopes EC, Cheema SS (2003) Neuromuscular accumulation of mutant superoxide dismutase 1 aggregates in a transgenic mouse of familial myotrophic lateral sclerosis. Neurosci Lett 350:132–136
52. Turner BJ, Atkin JD, Farg MA, Zang DW, Rembach A, Lopes EC, Patch JD, Hill AF, Cheema SS (2005) Impaired extracellular secretion of mutant superoxide dismutase 1 associates with neurotoxicity in familial amyotrophic lateral sclerosis. J Neurosci 25:108–117
53. Urushitani M, Kurisu J, Takahashi R (2002) Proteasomal inhibition by misfolded mutant superoxide dismutase 1 induces selective motor neuron death in familial amyotrophic lateral sclerosis. J Neurochem 83:1030–1042
54. Wang J, Xu G, Borchelt DR (2002) High molecular weight complexes of mutant superoxide dismutase 1: age-dependent and tissue specific accumulation. Neurobiol Dis 9:139–148
55. Watanabe M, Dykes-Hoberg M, Culotta VC, Price DL, Wong PC, Rothstein JD (2001) Histological evidence of protein aggregation in mutant SOD1 transgenic mice and in amyotrophic lateral sclerosis neural tissues. Neurobiol Dis 8:933–941
56. Wong PC, Pardo CA, Borchelt DR, Lee MK, Copeland NG, Jenkins NA, Sisodia SS, Cleveland DW, Price DL (1995) An adverse property of a familial ALS-linked SOD1 mutation causes motor neuron disease characterized by vacuolar degeneration of mitochondria. Neuron 14:1105–1116
57. Yamashita S, Mita S, Kato S, Okado H, Ohama E, Uchino M (2003) Bcl-2 expression using retrograde transporter of adenoviral vectors inhibits cytochrome *c*-release and caspase-1 activation in motor neurons of mutant superoxide dismutase 1 (G93A) transgenic mice. Neurosci Lett 350:17–20
58. Yang J, Liu X, Bhalla K, Kim CN, Ibrado AM, Cai J, Peng TI, Jones DP, Wang X (1997) Prevention of apoptosis by Bcl-2: release of cytochrome *c* from mitochondria blocked. Science 275:1129–1132

Rapid disease progression correlates with instability of mutant SOD1 in familial ALS

T. Sato, T. Nakanishi, Y. Yamamoto, P. M. Andersen, Y. Ogawa, K. Fukada, Z. Zhou, F. Aoike, F. Sugai, S. Nagano, S. Hirata, M. Ogawa, R. Nakano, T. Ohi, T. Kato, M. Nakagawa, T. Hamasaki, A. Shimizu and S. Sakoda

Neurology 2005;65;1954-1957; originally published online Nov 16, 2005;
DOI: 10.1212/01.wnl.0000188760.53922.05

HIGH LIGHT

Rapid disease progression correlates with instability of mutant *SOD1* in familial ALS

Abstract—Studies on the clinical course of familial ALS suggest that the duration of illness is relatively consistent for each mutation but variable among the different mutations. The authors analyzed the relative amount of mutant compared with normal SOD1 protein in the erythrocytes from 29 patients with ALS with 22 different mutations. Turnover of mutant SOD1 correlated with a shorter disease survival time.

NEUROLOGY 2005;65:1954–1957

T. Sato, MD*; T. Nakanishi, PhD*; Y. Yamamoto, MD, PhD; P.M. Andersen, MD, PhD; Y. Ogawa, MD, PhD; K. Fukada, MD, PhD; Z. Zhou, MD, PhD; F. Aoike, MD; F. Sugai, MD; S. Nagano, MD, PhD; S. Hirata, MD; M. Ogawa, MD, PhD; R. Nakano, MD, PhD; T. Ohi, MD, PhD; T. Kato, MD, PhD; M. Nakagawa, MD; T. Hamasaki, PhD; A. Shimizu, MD, PhD; and S. Sakoda, MD, PhD

One hundred fourteen different mutations have been reported in the Cu/Zn superoxide dismutase (*SOD1*) gene. The age at onset varies greatly among patients with ALS with a given mutation, but the duration of illness seems to be relatively consistent for a given mutation.[1,2] Therefore, the duration of illness is considered to be closely linked to some property of each mutant protein.

We devised a simple method to distinguish mutant SOD1 protein from normal SOD1 protein using liquid chromatography electrospray ionization mass spectrometry (LC-ESI-MS).[3] We found that the ratio of mutant/normal SOD1 protein was 0.60 in the diaphragm, 0.47 in the iliopsoas muscle, 0.43 in the spinal cord, and 0.14 in erythrocytes for the His46Arg mutant.[4] Because no protein synthesis occurs in the enucleated erythrocytes and the average cell age is 60 days, the instability of mutant SOD1 should be more apparent in erythrocytes compared with most other cells in the body.

We performed a systematic analysis of the relative amount of human mutant SOD1 proteins in erythrocytes in relation to the clinical course of ALS with 22 different *SOD1* gene mutations.

Methods. ALS was diagnosed according to the revised El Escorial criteria of the World Federation of Neurology. With informed consent, *SOD1* gene[2] and protein studies[3] were performed. The age at onset is the time of the first sign of muscle weakness, atrophy, or clinical symptoms involving upper or lower motor neurons. The duration of illness is the period from onset to respiratory failure. The protein analysis has been described.[3] The combined data from both dead and living patients were analyzed by log-normal regression using the EM algorithm, with the duration of illness as a response, and the ratio and age at onset as covariates.

Results. The *SOD1* gene and protein in erythrocytes of 29 patients with ALS and four carriers were analyzed by genomic sequencing and LC-ESI-MS. Twenty-seven patients presented with muscle weakness in their extremities, and 2 patients noticed dyspnea as the initial symptom of ALS. As representative data, transformed mass spectra of SOD1 protein from Patients 23 and 25 are shown in figure 1. The molecular masses of the peaks in figure 1, A and B, were 15846.2 Da and 15845.0 Da, which coincided with the theoretical average for the monomer of normal SOD1, 15844.6 Da. SOD1 from Patient 23 showed an ion peak of mutant SOD1 in addition to a normal peak (see figure 1A). The mutant peak had a molecular mass of 15820.7 Da, and the difference of 25.5 Da corresponded to the mutation from leucine to serine. In Patient 25, we could not detect any significant peaks except the normal peak (see figure 1B). We measured the intensities of the signals for SOD1 and mutant SOD1, and the results are shown in the table. The samples from Patients 14 and 15, whose ratios of mutant/normal SOD1 were 0.50 and 0.57, respectively, had been stored at −80 °C for 15 months and 5 years. Similarly, those from

This article was previously published in electronic format as an Expedited E-Pub on November 16, 2005, at www.neurology.org.

* These authors contributed equally to this work.

From the Department of Neurology (Drs. Sato, Yamamoto, Y. Ogawa, Fukada, Zhou, Aoike, Sugai, Nagano, and Sakoda), Department of Medical Statistics (Dr. Hamasaki), Osaka University Graduate School of Medicine, Suita, Osaka, Japan; Department of Clinical Pathology (Drs. Nakanishi and Shimizu), Osaka Medical College, Takatsuki, Osaka, Japan; Awaji Prefectural Hospital (Dr. Hirata), Sumoto, Hyogo, Japan; Aomori Prefectural Central Hospital (Dr. M. Ogawa), Aomori, Japan; Department of Neurology (Dr. Nakano), Brain Research Institute, Niigata University, Niigata, Japan; Division of Neurology (Dr. Ohi), Department of Internal Medicine, Miyazaki University School of Medicine, Miyazaki, Japan; Third Department of Internal Medicine (Dr. Kato), Yamagata University School of Medicine, Yamagata, Japan; Department of Neurology and Gerontology (Dr. Nakagawa), Research Institute for Neurological Diseases and Geriatrics, Kyoto Prefectural University of Medicine, Kyoto, Japan; and Department of Neurology (Dr. Andersen), Umeå University Hospital, Umeå, Sweden.

Supported by Grants-in-Aid for Scientific Research in Japan and by a grant on Specific Diseases (Y.I.) from the Ministry of Health and Welfare, Japan.

Disclosure: The authors report no conflicts of interest.

Received August 4, 2004. Accepted in final form September 1, 2005.

Address correspondence and reprint requests to Dr. Yoichi Yamamoto, Department of Neurology D4, Osaka University Graduate School of Medicine, 2-2 Yamada-oka, Suita, Osaka 565-0871, Japan; e-mail: yamamoto@neurol.med.osaka-u.ac.jp

Editorial, see page 1859

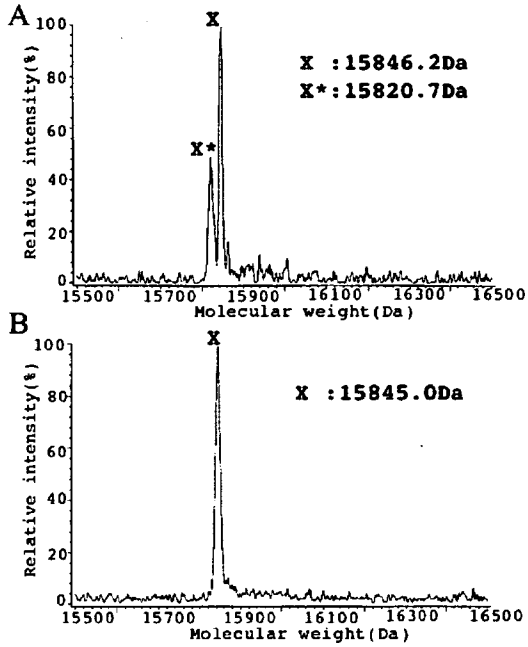

Figure 1. Transformed electrospray ionization (ESI) mass spectra of SOD1 prepared by immunoprecipitation from Patient 23 (A) and Patient 25 (B) listed in the table. X and X indicate normal and mutant monomer SOD1, respectively.*

Patients 33 and 18, whose ratios were 0.34 and 0.29, respectively, had been stored for 29 months and 5.6 years. These results indicated that the duration of preservation had little effect on the ratio. The ratios from three patients and two carriers with the Ala4Val mutation were not detected.

First, we found that the age at onset and the duration of illness were independent of each other ($p = 0.7157$). Next, we plotted the ratio of mutant/normal SOD1 against age at disease onset (figure 2A) or duration of illness (figure 2B). We found that the age at onset had no relationship with the ratio. Conversely, to assess the effects of covariates on the duration of illness, we performed the likelihood ratio test, and found that the effect of this ratio on the duration of illness was evident at the level of 5% ($p = 0.0029$; see figure 2B). In addition, to examine whether the survival time of the patient was longer or shorter if the ratio was greater or less than a certain value, the values of the Akaike Information Criterion (AIC), an index commonly used as an aid for choosing between competing models, were computed,[5] categorizing the value of the ratio into two groups. The value of AIC was the smallest when categorizing the ratio into two groups, not detected and detected (AIC = −55.312), and this suggests that the difference in the duration of illness is the largest between

Table *Summary of clinical features and mutant/normal SOD1*

Case	Sex	SOD1 mutation	Age at onset, y	Site of onset	Duration of illness	Mutant/normal SOD1
1	M	Ala4Ser	34	L leg	>3 y	0.56
2	M	Ala4Thr	21	L lower limb	20 mo	Not detected
3	M	Ala4Val	43	R hand	32 mo	Not detected
4	M	Ala4Val	60	R hand	7 mo	Not detected
5	F	Ala4Val	48	L arm	14 mo	Not detected
6	M	Val14Gly	41	Leg paresis	20 mo	0.33
7	M	Gly37Arg	41	R hand	6 y	0.56
8	M	Gly41Asp	36	R leg	>11 y	Not detected
9	F	His46Arg	59	R lower limb	5 y	0.11
10	M	His46Arg	46	L lower limb	>11 y	0.18
11	M	Asp76Tyr	49	R foot	17 y	0.61
12	F	Asn86Ser	36	L leg	9 y	0.12
13	M	Asn86Ser	63	R foot	6 y	0.12
14	M	Ala89Val	70	R foot	>35 mo	0.5
15	F	Ala89Val	55	L foot	>6 y	0.57
16	M	Asp101His	52	R hand	3 mo	Not detected
17	F	Ser105Leu	54	R arm	5 y	Not detected
18	F	Ile113Thr	63	L arm	19 mo	0.29
19	F	Ile113Phe	68	L leg	>6 y	0.23
20	M	Gly114Ala	38	L hand	29 mo	Not detected
21	M	Arg115Gly	66	L leg	>22 mo	Not detected
22	F	Leu1262bp del	42	R foot	17 mo	Not detected
23	M	Leu126Ser	63	Bilateral feet	>3 y	0.5
24	M	Gly127insTGGG	52	Bulbar	8 mo	Not detected
25	M	Ser134Asn	52	R upper limb	9 mo	Not detected
26	M	Ser134Asn	39	Bulbar	10 mo	Not detected
27	M	Gly141Glu	43	R leg	> 4 y	0.28
28	M	Leu144Phe	71	R leg	>12 mo	0.29
29	F	Leu144Phe	42	L foot	>3 y	0.29
30	M	Ala4Val	Unaffected			Not detected
31	F	Ala4Val	Unaffected			Not detected
32	F	Asp76Tyr	Unaffected			0.58
33	M	Ile113Thr	Unaffected			0.34

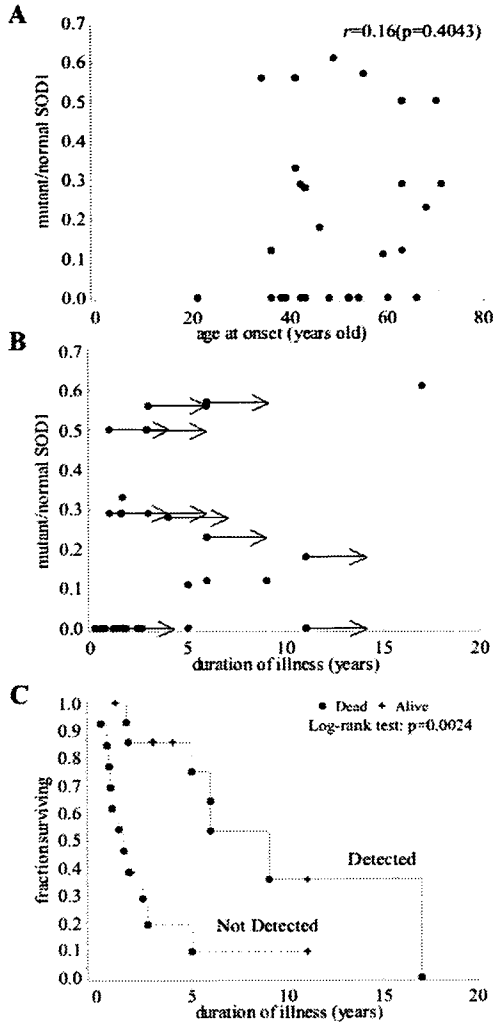

Figure 2. Ratio of mutant/normal SOD1 protein in erythrocytes plotted against clinical course. Ratio 0 indicates mutant protein was not detected. (A) Age at onset. (B) Duration of illness. Arrows designate that patients are alive. (C) Kaplan–Meier survival curve plot. Filled circles represent dead patients, and crosses represent living patients. Solid line and dashed line represent mutant SOD1 proteins that were detected or not detected, respectively. The median survival time was estimated as 1.4 years (95% CI 0.8 to 11.0 years) for the not-detected group and 9.0 years (95% CI 6.0 to 17.0 years) for the detected group. This curve shows that the survival curve for the detected group is always higher than that for the not-detected group. This means that patients in the detected group are alive longer than those in the not-detected group. The two groups did not contain the same type of mutation.

these two groups, as shown by the Kaplan–Meier survival curve plot (figure 2C).

Discussion. The stability of SOD1 mutant protein has been investigated using in vitro models. Unfolding transitions of purified SOD1 mutant holoproteins and apoproteins were examined. The results showed that patients with severe loss of stability of apo-SOD1 have a low mean survival time.[6] Based on the half-lives of the proteins estimated using transfection of plasmids encoding wild-type or mutant SOD1 into cell lines, it was reported that clinical progression was not correlated with the half-lives of the mutant SOD1 proteins.[7]

In mice transgenic for the Gly93Ala and Gly37Arg SOD1 mutations, a high copy number of the mutant *SOD1* gene was required for the development of motor neuron disease, indicating that a large amount of mutant SOD1 protein is necessary for the disease expression in these models. Conversely, in transgenic mice carrying Gly85Arg or Gly127insTGGG SOD1 and showing extremely rapid disease progression, the mutant protein was not detectable in erythrocytes and was barely detected in spinal cord extracts.[8,9] Using highly specific antibodies against the truncated Gly127insTGGG SOD1 mutant, it was shown that the amount of mutant SOD1 protein was less than 0.5% of that of the normal SOD1 protein in the brain and spinal cord of the patient. In addition, the immunohistopathologic study of the spinal cord of the patient revealed that motor neuron inclusions were labeled by antibody directed against ubiquitin and some were also labeled by the mutant-specific antibody. These results suggest that at least part of the SOD1 was degraded via a ubiquitin-dependent pathway.[9]

We previously classified SOD1 mutants into stable type (detected group in this study) and unstable type (not-detected group in this study).[10] The transgenic mice carrying stable-type SOD1 mutations (Gly93Ala and Gly37Arg) were reported to show vacuolation pathology, and those carrying unstable-type mutations (Gly85Arg and Gly127insTGGG) had Lewy body–like inclusions in motor neurons and astrocytes. Therefore, the stability of the SOD1 mutant proteins is deeply involved in not only the clinical course but also the pathology of familial ALS.

The not-detected group included an American patient with the Gly41Asp mutation who is currently alive with disease duration of 11 years. This indicates that although the stability of the mutant protein correlates well with the disease progression statistically, there might be other factors influencing the disease duration, at least for the Gly41Asp mutation. We analyzed erythrocytes from three patients and two carriers with the Ala4Val mutation, and the mutant protein was not detected in any of them. We also analyzed samples from one patient and one carrier each with the Asp76Tyr or Ile113Thr mutation and found that the ratios were 0.61 and 0.58 for the Asp76Tyr mutation or 0.29 and 0.34 for the Ile113Thr mutation (see table). Although the function of the synthesis and degradation of each mutant protein throughout life is still unknown, these results indicate that the ratio may not change during the course of the disease. Whether molecules that stabilize the unstable mutants could be useful for therapy for familial ALS remains to be tested.

References

1. Radunovic A, Leigh PN. Cu/Zn superoxide dismutase gene mutations in amyotrophic lateral sclerosis: correlation between genotype and clinical features. J Neurol Neurosurg Psychiatry 1996;61:565–572.
2. Andersen PM, Nilsson P, Keranen ML, et al. Phenotypic heterogeneity in motor neuron disease patients with CuZn-superoxide dismutase mutations in Scandinavia. Brain 1997;120:1723–1737.
3. Nakanishi T, Kishikawa M, Miyazaki A, et al. Simple and defined method to detect the SOD-1 mutants from patients with familial amyotrophic lateral sclerosis by mass spectrometry. J Neurosci Methods 1998;81:41–44.
4. Arisato T, Okubo R, Arata H, et al. Clinical and pathological studies of familial amyotrophic lateral sclerosis (FALS) with SOD1 H46R mutation in large Japanese families. Acta Neuropathol (Berl) 2003;106:561–568.
5. Akaike H. Information theory and an extension of the maximum likelihood principle. In: Petrov BN, Csaki F, eds. The 2nd International Symposium on Information Theory. Budapest, Akademi Kaido, 1972: 267–281.
6. Lindberg MJ, Tibell L, Oliveberg M. Common denominator of Cu/Zn superoxide dismutase mutants associated with amyotrophic lateral sclerosis: decreased stability of the apo state. Proc Natl Acad Sci USA 2002;99:16607–16612.
7. Ratovitski T, Corson LB, Strain J, et al. Variation in the biochemical/biophysical properties of mutant superoxide dismutase 1 enzymes and the rate of disease progression in familial amyotrophic lateral sclerosis kindreds. Hum Mol Genet 1999;8:1451–1460.
8. Bruijn LI, Becher MW, Lee MK, et al. ALS-linked SOD1 mutant G85R mediates damage to astrocytes and promotes rapidly progressive disease with SOD1-containing inclusions. Neuron 1997;18:327–338.
9. Jonsson PA, Ernhill K, Andersen PM, et al. Minute quantities of misfolded mutant superoxide dismutase-1 cause amyotrophic lateral sclerosis. Brain 2004;127:73–88.
10. Fukada K, Nagano S, Satoh M, et al. Stabilization of mutant Cu/Zn superoxide dismutase (SOD1) protein by coexpressed wild SOD1 protein accelerates the disease progression in familial amyotrophic lateral sclerosis mice. Eur J Neurosci 2001;14:2032–2036.

THE JOURNAL OF BIOLOGICAL CHEMISTRY VOL. 282, NO. 49, pp. 35933–35944, December 7, 2007

Oxidative Modification to Cysteine Sulfonic Acid of Cys^{111} in Human Copper-Zinc Superoxide Dismutase*[S]

Received for publication, April 6, 2007, and in revised form, August 31, 2007 Published, JBC Papers in Press, October 3, 2007, DOI 10.1074/jbc.M702941200

Noriko Fujiwara[‡1,2], **Miyako Nakano**[§1], **Shinsuke Kato**[¶], **Daisaku Yoshihara**[‡], **Tomomi Ookawara**[‡], **Hironobu Eguchi**[‡], **Naoyuki Taniguchi**[‖], **and Keiichiro Suzuki**[‡]

From the [‡]Department of Biochemistry, Hyogo College of Medicine, Nishinomiya, Hyogo, 663-8501, Japan, the [§]Department of Biochemistry, Osaka University Medical School and Graduate School of Medicine, Suita, Osaka, 565-0871, Japan, the [¶]Department of Neuropathology, Institute of Neurological Sciences, Faculty of Medicine, Tottori University, Nishi-cho 36-1, Yonago 683-8504, Japan, and the [‖]Department of Disease Glycomics, Research Institute for Microbial Diseases, Osaka University, Suita, Osaka 565-0871, Japan

Copper-zinc superoxide dismutase (SOD1) plays a protective role against oxidative stress. On the other hand, recent studies suggest that SOD1 itself is a major target of oxidative damage and has its own pathogenicity in various neurodegenerative diseases, including familial amyotrophic lateral sclerosis. Only human and great ape SOD1s among mammals have the highly reactive free cysteine residue, Cys^{111}, at the surface of the SOD1 molecule. The purpose of this study was to investigate the role of Cys^{111} in the oxidative damage of the SOD1 protein, by comparing the oxidative susceptibility of recombinant human SOD1 modified with 2-mercaptoethanol at Cys^{111} (2-ME-SOD1) to wild-type SOD1. Wild-type SOD1 was more sensitive to oxidation by hydrogen peroxide-generating fragments, oligomers, and charge isomers compared with 2-ME-SOD1. Moreover, wild-type SOD1, but not 2-ME-SOD1, generated an upper shifted band in reducing SDS-PAGE even by air oxidation. Using mass spectrometry and limited proteolysis, this upper band was identified as an oxidized subunit of SOD1; the sulfhydryl group (Cys-SH) of Cys^{111} was selectively oxidized to cysteine sulfinic acid (Cys-SO_2H) and to cysteine sulfonic acid (Cys-SO_3H). The antibody raised against a synthesized peptide containing Cys^{111}-SO_3H reacted with only the Cys^{111}-peroxidized SOD1 by Western blot analysis and labeled Lewy body-like hyaline inclusions and vacuole rims in the spinal cord of human SOD1-mutated amyotrophic lateral sclerosis mice by immunohistochemical analysis. These results suggest that Cys^{111} is a primary target for oxidative modification and plays an important role in oxidative damage to human SOD1, including familial amyotrophic lateral sclerosis mutants.

Copper-zinc superoxide dismutase (Cu/Zn-SOD)[3] (SOD1) is a homodimer containing one copper ion and one zinc ion in each 16-kDa subunit. SOD1 catalyzes the conversion of superoxide anion (O_2^-) into O_2 and H_2O_2, thereby protecting cells against oxidative stress. On the other hand, SOD1 exhibits peroxidase activity and oxidizes various substrates in the presence of hydrogen peroxide, H_2O_2 (1). Although H_2O_2 is a substrate as well as a product of SOD1, incubation of bovine SOD1 with H_2O_2 caused oxidation of His^{118} (corresponding to His^{120} in human SOD1) to 2-oxohistidines, inactivating the enzyme (2). Moreover, incubation with excess H_2O_2 caused oxidation of almost all histidine and cysteine residues (3), fragmentation (4, 5) and aggregation (6, 7) of SOD1 itself. Co-incubation with bicarbonate and H_2O_2 also induced bicarbonate radical anion formation, resulting in oligomerization of human SOD1 (8).

The familial form of amyotrophic lateral sclerosis (ALS) is associated with specific mutations in the SOD1 gene (*SOD1*) that encodes 153 amino acids (9, 10). To date, more than 110 familial ALS (FALS)-causing mutations in SOD1 have been identified (available on the World Wide Web); however, the mechanism by which SOD1 mutants induce ALS remains unknown. The presence of intracellular aggregates that contain SOD1 in spinal cord motor neurons is thought to be a pathological hallmark of ALS. In particular, FALS-linked mutant SOD1s are prone to misfolding and aggregation (11, 12). Recently, Ezzi *et al.* (7) reported that even wild-type SOD1 results in aggregation after oxidation, and the oxidized wild-type SOD1 gains properties like FALS mutant SOD1s. In addition to ALS, oxidative damaged SOD1 proteins were detected in the brains of patients with Alzheimer and Parkinson diseases (13). These findings suggest that oxidized SOD1 plays a role in the pathophysiology of various neurodegenerative diseases.

* This work was supported by Grants-in-aid for Scientific Research 17500242 and 19500313; a Hitech Research Center grant and the 21st Century Centers of Excellence program from the Ministry of Education, Culture, Sports, Science and Technology of Japan; and in part by a Grant for the Research Group on Development of Novel Therapeutics for ALS from the Ministry of Health, Labor and Welfare of Japan. The costs of publication of this article were defrayed in part by the payment of page charges. This article must therefore be hereby marked "*advertisement*" in accordance with 18 U.S.C. Section 1734 solely to indicate this fact.

[S] The on-line version of this article (available at http://www.jbc.org) contains supplemental Figs. 1 and 2.

[1] These authors contributed equally to this work.

[2] To whom correspondence should be addressed. Tel.: 81-798-45-6357; Fax: 81-798-46-3164; E-mail: noriko-f@hyo-med.ac.jp.

[3] The abbreviations used are: SOD, superoxide dismutase; ALS, amyotrophic lateral sclerosis; FALS, familial amyotrophic lateral sclerosis; MALDI, matrix-assisted laser desorption/ionization; TOF, time of flight; ESI, electrospray ionization; MS, mass spectrometry; MS/MS, tandem MS; TBS, Tris-buffered saline; PVDF, polyvinylidene fluoride; DTT, dithiothreitol; 2-ME, 2-mercaptoethanol; IA, iodoacetamide; HPLC, high performance liquid chromatography; PBS, phosphate-buffered saline; ELISA, enzyme-linked immunosorbent assay; Prx, peroxiredoxin; BSA, bovine serum albumin; CHAPS, 3-[(3-cholamidopropyl)dimethylammonio]-1-propanesulfonic acid; IPG, immobilized pH gradient; LBHI, Lewy body-like hyaline inclusion.

However, the role of oxidized wild-type and FALS-linked mutant SOD1s on these diseases remains unclear.

Human SOD1 has four cysteine residues, Cys^6, Cys^{57}, Cys^{111}, and Cys^{146}. An internal disulfide bond exists between Cys^{57} and Cys^{146} (14, 15), which contributes to the high stability of the SOD1 protein. This disulfide bond is highly conserved in SOD1s from various organisms, including yeast, plants, flies, fishes, and mammals. In contrast, two free cysteines, Cys^6 and Cys^{111}, are not conserved. Actually, yeast, fungi, and spinach (plants) have no free cysteines, and residue 6 is Ala and residue 111 is Ser in these organisms (16). More evolved organisms, such as flies, fishes, and mammals, including the Japanese monkey, have only one free cysteine, Cys^6. Only humans and great apes (chimpanzee and orangutan) have two free cysteines, Cys^6 and Cys^{111} (17). Notably, the amino acid sequence of chimpanzee SOD1 is identical to that of human SOD1. Although the evolutionary process may differ from humans and great apes, chicken SOD1 has three free cysteines, including Cys^6 and Cys^{111}. The third free Cys residue is located at the C terminus, Cys^{154} (18). Because free cysteines are generally reactive, and wild-type SOD1 is less thermo-stable than Ser^{111}-SOD1 or Ala^6-SOD1 (19), the A6C and S111C mutations during evolution are puzzling. In particular, Cys^{111} is located at the surface of the SOD1 molecule and is thought to be highly reactive. De Beus *et al.* (20) reported that Cys^{111} was modified with persulfide (S-SH) in a human SOD1 isolated from erythrocytes that is commercially available (Sigma). The persulfide SOD1 was more resistant to copper-induced aggregation than wild-type SOD1 (20). The sulfur atom of cysteine is able to assume several different oxidation states. Reversible oxidation of cysteine to disulfide (-S-S-) or sufenic acid (-SOH) is readily accomplished by thiols, such as DTT, 2-ME, glutathione, or thioredoxin. In contrast, oxidation to sulfinic acid ($-SO_2H$) or sulfonic acid ($-SO_3H$) is not reduced by these thiols under physiological conditions (21). For example, one cysteine in the active site of peroxiredoxin (Prx) is oxidized to sulfinic acid ($-SO_2H$) by incubation with an excess of substrate of this enzyme, H_2O_2, and rereduced by a specific enzyme, sulfiredoxin, but not by general thiols (22, 23).

An upper shifted band of human wild-type or mutant SOD1s, with the exception of mutant C111S, on SDS-PAGE has been observed under a variety of conditions: during purification (24) or when hydrogen peroxide or copper ion is added (see Fig. 1). The SOD1 in the upper band is speculated to be irreversibly linked to another molecule via a covalent bond at Cys^{111}; however, neither the molecule nor the modification site have been identified. Ube Industries Ltd. developed recombinant human SOD1 chemically modified with 2-mercaptoethanol at Cys^{111} (2-ME-SOD1; Cys^{111}-S-S-CH_2CH_2OH). This 2-ME-SOD1 is stable for many years in aqueous solution, showing neither degradation nor a loss of activity. Thus, in this study, the role of Cys^{111} in oxidative damage of human SOD1 was investigated by comparing 2-ME-SOD1 and wild-type SOD1, and the identity of the molecule that is bound to human SOD1 in the upper band on SDS-PAGE was explored. Through mass spectrometry and limited proteolysis, it was determined that the mass size of the molecule is 32 and 48 and that the modification site in SOD1 is Cys^{111}. We demonstrated that Cys^{111} in human SOD1 is selectively oxidized to cysteine sulfinic acid (Cys-SO_2H) and to cysteine sulfonic acid (Cys-SO_3H) even by air oxidation. Moreover, a polyclonal antibody was raised against a synthesized peptide containing Cys^{111}-SO_3H. This antibody, denoted as anti-C111ox-SOD1, reacted with the upper band (oxidized SOD1) but not the original band by Western blot analysis. Using this anti-C111ox-SOD1, the role of Cys^{111} on the generation of SOD1 charge isomers and the presence of oxidized SOD1 in the spinal cord of ALS mice were investigated.

EXPERIMENTAL PROCEDURES

Materials—All chemicals used in this study were obtained either from Wako Pure Chemical Industries Ltd. (Osaka, Japan), Nacalai Tesque, Inc. (Kyoto, Japan), or Sigma unless specified otherwise. Recombinant human SOD1, chemically modified with 2-mercaptoethanol (2-ME-SOD1), was kindly provided from Ube Industries Ltd. Horseradish peroxidase-conjugated goat anti-rabbit IgG and horseradish peroxidase-conjugated rabbit anti-goat IgG were purchased from Dako (Denmark). Lysylendopeptidase (Achromobacter Proteinase I) was obtained from Wako Pure Chemical Industries Ltd. (Osaka, Japan). Sequencing grade modified trypsin was purchased from Promega (Madison, WI). Sinapinic acid and α-cyano-4-hydroxycinnamic acid for matrix of MALDI-TOF MS were obtained from Bruker Daltonik GmbH (Bremen, Germany).

Conversion of 2-ME-SOD1 to Wild-type SOD1—2-ME-SOD1 was incubated with 20 mM 2-ME for 1 h on ice and desalted with a PD-10 column. The resultant wild-type SOD1 and 2-ME-SOD1 were used in the experiments with the exception of the experiments in Fig. 1, *B* and *C*.

Production and Purification of Wild-type and Mutant SOD1 Proteins—Overproduction of SOD1s by the baculovirus/insect cells system and purification of SOD1 proteins were carried out as described previously (25).

Oxidation of SOD1 and the Analyses with MonoQ Column—For strong oxidation, SOD1s diluted with miliQ water (1 mg/ml) were incubated with 5 mM H_2O_2 for 1 h at room temperature. For mild air oxidation, SOD1s diluted with miliQ water or appropriate buffer were filtered with a 0.22-μm filter (Millipore) and were slowly stirred at 30 rpm with a rotator (rotator RT-50; Taitec). The buffer or water containing oxidized SOD1s was changed with buffer A (2 mM potassium phosphate, pH 7.4) on a PD-10 column (Amersham Biosciences). The SOD1s were applied to a high performance liquid chromatograph (AKTA Explorer 10S) at a flow rate of 1 ml/min on a MonoQ column (MonoQ™ 4.6/100 PE; Amersham Biosciences). After washing with buffer A, the bound proteins were eluted with a linear gradient of KCl (0–100 mM) in buffer A. Adhesive proteins were washed with 0.5 M KCl in buffer A.

Lysylendopeptidase Treatment and Peptide Analyses—SOD1 proteins were reduced with DTT, and the free sulfhydryls were carbamidemethylated by adding iodoacetamide (IA) in the dark at room temperature for 30 min. After desalting on a PD-10 column with 50 mM Tris-HCl (pH 8.8), the proteins were digested with 0.25% (w/w) lysylendopeptidase (Wako Pure Chemicals) at 37 °C for 16 h. The resultant peptides were applied to a reverse-phase high performance liquid chromato-

graph (AKTA Explorer 10S) at a flow rate of 1 ml/min on TSK-GEL ODS-80TM (4.6 × 250 mm; Tosoh). The peptides were separated by two linear gradients of 0–30% acetonitrile for 4 column volumes and 30–40% acetonitrile for 8 column volumes containing 0.05% trifluoroacetic acid. Peptides were detected by their absorbance at 215 nm. The peaks were subjected to the following MS analyses.

MALDI-TOF MS Analysis—MALDI-TOF MS spectra of peptides and proteins were measured on an Ultraflex TOF/TOF mass spectrometer and analyzed by the Flexcontrol 1.2 software package (Bruker Daltonics GmbH, Bremen, Germany). For analyses of peptides, ions generated by a pulsed UV laser beam (nitrogen laser; λ = 337 nm, 5 Hz) were accelerated to a kinetic energy of 20 kV in reflector mode using positive polarity. Metastable ions generated by laser-induced decomposition of the selected precursor ions were analyzed without any additional collision gas. α-Cyano-4-hydroxycinnamic acid (5 mg/ml in 50% acetonitrile containing 0.1% trifluoroacetic acid) was used as a matrix for peptide analyses. For analyses of proteins, the determinations were performed in linear mode using positive polarity. Sinapinic acid (10 mg/ml in 50% acetonitrile containing 0.1% trifluoroacetic acid) was used as matrix for protein analyses. Peptide or protein samples (1 μl each) were mixed with matrix solution (4 μl each), and an aliquot (1 μl each) was applied to a polished stainless steel target (Bruker Daltonics). The mixture was dried in air at room temperature for several minutes.

Infusion ESI MS Analysis for Peptide Sequence—ESI mass spectra were measured on a Bruker Esquire HCT equipped with a quadrupole ion trap (Bruker Daltonics GmbH, Bremen, Germany). The solutions containing peptides digested with lysylendopeptidase were continuously introduced through the electrospray interface with a syringe infusion pump (Cole-Parmer, Vernon Hills, IL) at a flow rate of 5 μl/min. The MS conditions were as follows: nebulizer gas (N_2), 10 p.s.i.; dry gas (N_2), 4 liters/min; dry temperature, 250 °C; capillary voltage, 3500 V; high voltage end plate offset, −500 V; capillary exit, 190.6 V; skimmer, 40 V; trap drive, 166.7. MS/MS spectra were sequenced using BioTool 2.2 software and Sequence editor 2.2 (algorithm provided by Bruker).

Trypsin Digestion for MALDI-TOF MS—SOD1 proteins in 50 mM NH_4HCO_3 were digested with trypsin at 37 °C for 16 h. An aliquot of the digests (10 μl) was boiled, applied to ZipTip C18 P10 (Millipore, Bedford, MA; according to the manufacturer's protocol) for desalting, and then subjected to MALDI-TOF MS analysis. When alkylation is needed, SOD1 proteins in 50 mM NH_4HCO_3 were treated with excess IA in the dark at room temperature for 30 min before trypsin digestion.

In-gel Digestion of Coomassie Brilliant Blue-stained Polyacrylamide Gel for MALDI-TOF MS—The gel bands containing SOD1 protein after SDS-PAGE were clipped out and cut into small pieces in a 1.5-ml microtube. To remove Coomassie Brilliant Blue dye, the chopped gels were washed three times with 50 mM NH_4HCO_3 in 30% acetonitrile by shaking at room temperature for 20 min. The gels were further incubated with 500 μl of acetonitrile at room temperature for 10 min. After removing acetonitrile, the gels were incubated with an alkylating solution (500 μl) consisting of 40 mM IA, 10 mM EDTA, and 50 mM NH_4HCO_3 in the dark at room temperature for 30 min. After washing twice with 50 mM NH_4HCO_3 (500 μl) for 10 min, the gels were incubated with 0.4 μg of trypsin in 50 mM NH_4HCO_3 at 37 °C overnight. After removing the pieces of gels, the remained solution was concentrated with a SpeedVac concentrator and subjected to MALDI-TOF MS analyses.

Preparation of Antibody for Cys^{111}-sulfonylated SOD1—Keyhole limpet hemocyanin-coupled peptide (residues 103–114) containing sulfonylated Cys^{111} (Cys^{111}-SO_3H) was obtained from Sigma. After the initial injection with the peptide-hemocyanin conjugate (200 μg of peptide) mixed with complete Freund's adjuvant, rabbits were subjected to five booster injections, each of 200 μg of peptide with incomplete Freund's adjuvant, administered (at multiple subcutaneous sites) at 1–2-week intervals. Antisera were collected 1 week after the sixth booster injection, and the IgG fraction was precipitated with 50% (w/v) ammonium sulfate. The IgG fraction passed from the wild-type SOD1 coupled to *N*-hydroxysucinimide-activated Sepharose was bound to the oxidized SOD1 coupled to *N*-hydroxysucinimide-activated Sepharose. The bound IgG was eluted with 3 M $MgCl_2$ and collected. The IgG was desalted with a PD-10 column and stored with 0.1 mg/ml bovine serum albumin (BSA) at deep freeze until use. This antibody was denoted as anti-C111ox-SOD1.

SDS-PAGE and Western Blot Analysis—Proteins were subjected to SDS-PAGE (14% gel) and then transferred to a PVDF membrane under semidry conditions by means of a Trans-blot (Bio-Rad). After blocking by incubation with 5% skim milk in Tris-buffered saline (TBS; 20 mM Tris-HCl, pH 8.0, 0.15 M NaCl) for 2 h at room temperature, the membrane was incubated with anti-C111ox-SOD1 (diluted 1:1000), or a goat polyclonal antibody against full-length human SOD1 (25), anti-SOD1 (diluted 1:1000), in TBS containing 0.05% Tween 20 (TBS-T) and 1% skim milk for 2 h at room temperature or for 18 h at 4 °C. After washing with TBS-T, the membrane was incubated with horseradish peroxidase-conjugated anti-rabbit IgG (diluted 1:5000) for anti-C111ox-SOD1 or horseradish peroxidase-conjugated anti-goat IgG (diluted 1:5000) in TBS-T containing 1% skim milk for anti-SOD1, respectively, for 2 h at room temperature. After washing, the chemiluminescence method using an ECL or an ECL plus kit (GE Healthcare) was employed to detect peroxidase activity.

Two-dimensional Gel Electrophoresis—Sample proteins were dissolved in 8 M urea, 2% (w/v) CHAPS, 0.5% (v/v) immobilized pH gradient (IPG) buffer (GE Healthcare), and 12 μl/ml DeStreak™ reagent (GE Healthcare), which forms stable disulfide bonds and prevents nonspecific Cys residue oxidation during isoelectric focusing (26). The samples were applied to 11-cm IPG strips (pH 4–7), and the strips were then isoelectrically focused on an IPGphor isoelectric focusing system (GE Healthcare) according to the following schedule: 500 V-h at 500 V for step and hold, 800 V-h at 1000 V for gradient, 8800 V-h at 6000 V for gradient, and 4000 V-h at 6000 V for step and hold. The strips were equilibrated for 20 min in 50 mM Tris-HCl (pH 8.8) containing 6 M urea, 2% (w/v) SDS, 30% (v/v) glycerol, and 1% (w/v) DTT. Second dimension separation was run on 14% SDS-polyacrylamide gels and followed by Western blot analysis. pI values of spots were calculated according to the graph

showing pH as function of distance at 20 °C and 8 M urea of IPG strips (pH 4–7) provided by the GE Healthcare on-line system.

ELISA—Wild-type SOD1 was air-oxidized, treated with and without 100 mM IA, and then diluted to 500 ng/ml with phosphate-buffered saline (PBS). 100 μl of the samples were added to each well of 96-well microplates (Maxisorp; Nunc), incubated overnight at 4 °C, washed three times with TBS-T, and then blocked for 2 h at room temperature with 1% BSA in PBS. The plates were then washed three times with TBS-T, and 100 μl of anti-C111ox-SOD1 and anti-SOD1 antibodies (diluted 1:1000 in TBS-T) was added, followed by incubation for 1 h at room temperature. The plates were washed three times with TBS-T, and 100 μl of horseradish peroxidase-conjugated anti-rabbit IgG (diluted 1:5000 in TBS-T) for anti-C111ox-SOD1 or horseradish peroxidase-conjugated anti-goat IgG (diluted 1:5000 in TBS-T) for anti-SOD1, respectively, was added and incubated for 1 h at room temperature. After washing five times with TBS-T, the plates were developed using 100 μl of *o*-phenylenediamine dihydrochloride solution, and the reaction was stopped with 25 μl of 2 M HCl. The absorbance of each well was determined at 490 nm with a SPECTRAmax PLUS384 (Molecular Devices).

Animals and Animal Tissue Preparation—Four transgenic mice carrying a high copy number of the human G93A SOD1 gene (B6SJL-TgN[SOD1-G93A]1Gur, G1H-G93A) mice, were purchased from the Jackson Laboratory (Bar Harbor, ME). Two age-matched littermates were used as controls. All animals were handled in accordance with the guidelines for care and use (Tottori University). All four G1H-G93A mice at 110 days of age neurologically exhibited hind limb paralysis, and two littermate mice at 110 days of age did not show any clinical symptoms. The G1H-G93A and littermate mice were euthanized at 110 days of age. Animals were deeply anesthetized with sodium pentobarbital (0.1 ml/100 g of body weight). After perfusion of three G1H-G93A and two littermate mice via the aorta with PBS at 37 °C, they were fixed by perfusion with 4% paraformaldehyde in 0.1 M cacodylate buffer (pH 7.3). The spinal cords were removed and then postfixed in the same solution. The spinal cord of one mouse for Western blot analysis was removed after perfusion with PBS, quickly frozen in liquid nitrogen, and stored at −80 °C until use.

Protein Extraction from G1H-G93A Mouse Spinal Cord—The G1H-G93A spinal cord was homogenized in ice-cold homogenization buffer, 20 mM Tris-HCl (pH 6.8) containing Complete™ miniprotease inhibitor mixture (Roche Applied Science), and 100 mM IA for preventing the secondary oxidation of SH groups. The sample was centrifuged at 17,000 × *g* at 4 °C for 30 min, and the pellet was homogenized in the ice-cold homogenization buffer containing 1% Triton X-100. The sample was centrifuged at 17,000 × *g* at 4 °C for 30 min, the pellet was further homogenized in the ice-cold homogenization buffer containing 1% Triton X-100 and 2% SDS, and the sample was centrifuged at 17,000 × *g* at 4 °C for 30 min. The supernatants of each homogenization, buffer-soluble, Triton X-100-soluble, and SDS-soluble fractions, were subjected to SDS-PAGE and Western blot analyses.

Immunohistochemical Analysis—After fixation, the specimens were embedded in paraffin, cut into 5-μm-thick sections, and examined for immunohistochemical analysis. Sections were deparaffinized and then washed in PBS. Normal serum homologous with the secondary antibody diluted in 1% BSA-containing PBS (BSA-PBS) was used as a blocking reagent. Tissue sections were incubated with anti-C111ox-SOD1 (diluted 1:1000 in BSA-PBS) at 4 °C for 18 h. Bound antibody was visualized by the avidin-biotin-immunoperoxidase complex (ABC) method using the appropriate Vectastain Elite ABC rabbit IgG kit (Vector Laboratories) and 3,3′-diaminobenzidine tetrahydrochloride (Wako, Osaka, Japan) as a chromogen. The endogenous peroxidase activity was quenched by incubation for 30 min with 3% H_2O_2 after the secondary antibody treatment to prevent nonspecific oxidation before anti-C111ox-SOD1 treatment.

SOD1 Activity—SOD1 activity was assayed using the xanthine-xanthine oxidase/cytochrome *c* system as described previously (27).

Protein Assay—SOD1 protein concentrations were estimated using a dimeric molar extinction at 280 nm of 10,800 M^{-1} cm^{-1} (28). Protein concentrations of crude samples were determined using a BCA™ protein assay kit (Pierce) with BSA as a standard.

RESULTS

2-ME-SOD1 Obtained from Ube Industries Ltd. Was Modified with 2-ME Only at Cys^{111}—First, the chemical modification with 2-mercaptoethanol of recombinant human Cu/Zn-SOD (2-ME-SOD1) was confirmed. The molecular mass of 2-ME-SOD1 was determined to be 15,865.5 (supplemental Fig. S1*A*) to 15,871 *m/z* (supplemental Fig. S2*A*), which suggested the presence of 2-ME (76 Da) in apo-human SOD1 (monoisotopic mass, 15,794.86; average mass, 15,804.55). The metals, copper and zinc, of SOD1 were removed during MALDI-TOF MS analysis. Since this recombinant human SOD1 was expressed in *Escherichia coli*, the N terminus was not acetylated. To demonstrate that the 2-ME-SOD1 was in fact modified with 2-ME only at Cys^{111}, the 2-ME-SOD1 was digested with trypsin and then analyzed by MALDI-TOF MS and MS/MS. The mass of the tryptic peptide (2533 *m/z*) indicating residues Asp^{92}–Arg^{115} (2457 *m/z*) plus the mass of 2-ME (76 Da) (supplemental Fig. S1*B*) was analyzed by the collision-induced MS/MS. As shown in supplemental Fig. S1*C*, the major fragment ions, y4 (457.1 *m/z*), y5 (635.9 *m/z*), y6 (772.9 *m/z*), y14 (1530.9 *m/z*), y19 (2074.4 *m/z*), and y23 (2418.7 *m/z*), indicated the presence of 2-ME at Cys111. The mass of the tryptic peptide (933 *m/z*, missed cleavages = 1), residues Ala^1–Lys^9, indicated that another free cysteine, Cys^6, was not modified with 2-ME (supplemental Fig. S1*B*). MS/MS analyses of the residues Ala^1-Lys^9 also indicated that 2-ME was not contained in this peptide (supplemental Fig. S1*D*). These results demonstrated that Cys^{111}, but not Cys^6, was modified with 2-ME. The commercial human SOD1 from Sigma, modified with persulfide (S-SH) or with trisulfide (-S-S-S-) intersubunit linkage at Cys^{111}, exhibits an absorbance peak at 325 nm (20, 29). However, 2-ME-SOD1 did not exhibit the 325 nm peak (data not shown).

Additional 2-ME Treatment Recovered the 2-ME-SOD1 to Wild-type SOD1—Next, the ability to remove 2-ME from Cys^{111} was examined. 2-ME-SOD1 was incubated with 0 (H_2O), 2, 20, and 200 mM 2-ME for 1 h on ice; the excess 2-ME was removed on a PD-10 column with miliQ water, and then the mass of the proteins was analyzed. As shown in supplemental Fig. S2*A*, the incubation with more than 20 mM 2-ME decreased the mass of the protein (from 15,871 to 15,795 *m/z*). The difference in the mass was 76 m/z, indicating that incubation with 20 mM 2-ME removes 2-ME from Cys^{111}. Thus, to confirm this finding, the 2-ME-treated SOD1s were digested with trypsin after incubation with IA, and the mass of the resulting peptides was determined. Removal of 2-ME from Cys^{111}, would allow the SH group of Cys^{111} to be carbamidemethylated by IA, yielding a mass of 2514 (2456 plus 58) *m/z*. As shown in supplemental Fig. S2*B*, the mass of the tryptic peptide containing Cys^{111} (residues Asp^{92}–Arg^{115}) treated with more than 20 mM 2-ME was 2514 *m/z*. In contrast, the mass of the 2-ME-SOD1 treated with H_2O was 2533 *m/z*, indicating that the SH group of Cys^{111} remained bound to 2-ME. These results show that incubation of 2-ME-SOD1 with 2-ME in excess of 20 mM removed 2-ME from Cys^{111}, converting 2-ME-SOD1 to wild-type SOD1. The SOD activities of 2-ME-SOD1 and the wild-type SOD1 were 4181 and 4056 units/mg, respectively, indicating that both SOD1s have similar activities.

Upper Band of Oxidized Human SOD1 on SDS-PAGE Involves Cys^{111}—2-ME-SOD1 and wild-type SOD1 were incubated with various concentrations of H_2O_2 for 20 min and then subjected to reducing SDS-PAGE. Although 2-ME-SOD1 was slightly affected by H_2O_2 treatment, wild-type SOD1 showed an additional upper band when incubated with more than 1 mM H_2O_2 (Fig. 1*A*). When commercial gradient gels (5–20%, e-PAGEL; Atto) were used for the SDS-PAGE, the upper band was not observed (data not shown). It is thought that the two bands are unable to separate on the gradient gels. Next, various purified wild-type and mutant human SOD1 proteins expressed in the baculovirus/insect cell system (25) were oxidized with 1 mM H_2O_2, followed by reducing SDS-PAGE and Western blotting. As shown in Fig. 1*B*, the additional upper band appeared in all SOD1s, except C111S, after oxidation. Furthermore, the effects of various metal ions on the generation of the upper band were investigated. Only the Cu^{2+} ion, among all metal ions examined, formed an upper band similar to that observed after oxidation with H_2O_2 (Fig. 1*C*). Although Fe^{3+} and Fe^{2+} are thought to be oxidants, neither Fe^{3+} (data not shown) nor Fe^{2+} treatment generated the upper band. Next, wild-type SOD1 diluted with various pH buffers was slowly stirred (30 rpm with a rotator) for 24 h at room temperature. As shown in Fig. 1*D*, the upper band was generated when the pH of the incubation buffer was higher than pH 7. These results indicated that Cys^{111} was readily oxidized by oxygen in ambient air and that the sulfhydryl group (SH) of Cys^{111} was needed to provide a thiolate anion (S^-) for the oxidative modification.

Role of Cys^{111} in the Generation of Negatively Charged Molecules after Oxidation—To examine the role of Cys^{111} in the generation of negatively charged molecules after oxidation, 2-ME-SOD1 and wild-type SOD1 were incubated with 5 mM H_2O_2 for 1 h and were applied to a MonoQ column. Some of the

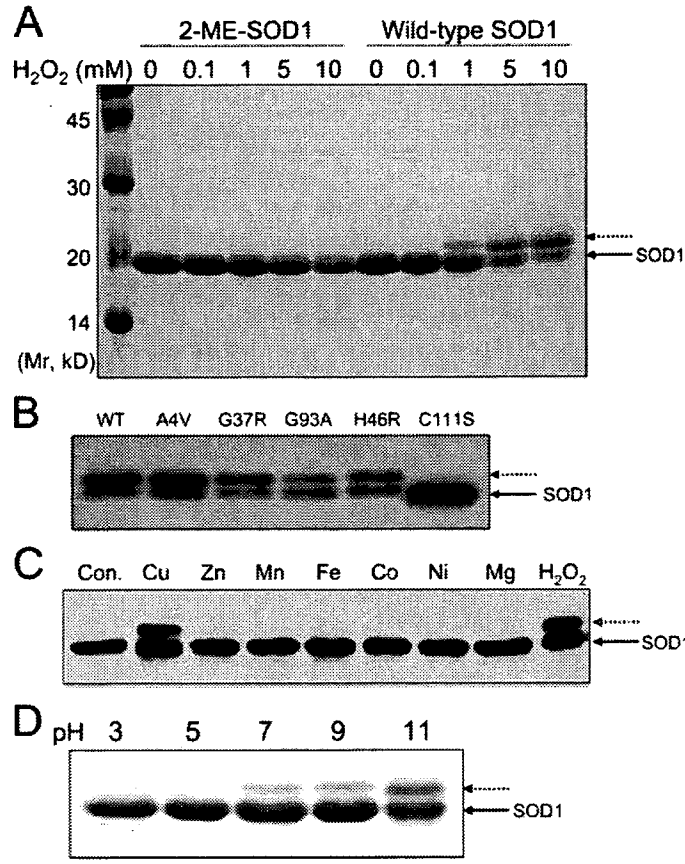

FIGURE 1. **Generation of upper shifted band of SOD1 on SDS-PAGE under reducing conditions.** *A*, 2-ME-SOD1 and wild-type SOD1 treated with various concentrations of H_2O_2 for 20 min, diluted with miliQ water, and boiled with SDS-PAGE loading buffer containing 5% 2-ME. 5 μg of protein/lane was subjected to SDS-PAGE (14% gel). Rainbow™ colored protein molecular weight markers purchased from GE Healthcare were used as molecular weight markers (*left*). *B*, Western blot analyses of wild-type and mutant SOD1s treated with 1 mM H_2O_2 for 20 min. *C*, Western blot analyses of wild-type SOD1 treated with 1 mM $CuCl_2$, $ZnCl_2$, $MnCl_2$, $FeCl_2$, $CoCl_2$, $NiSO_4$, $MgCl_2$, and H_2O_2 for 1 h. Wild-type and mutant SOD1s used in *B* and *C* were produced by the baculovirus/insect cells system. SOD1 proteins in *B* and *C* were immunostained with anti-SOD1. *D*, SDS-PAGE of wild-type SOD1 stirred for 24 h in various pH buffers (50 mM), citric acid-NaOH (pH 3.0), sodium citrate-disodium phosphate-NaOH (pH 5.0), sodium phosphate (pH 7.0), and glycine-NaOH (pH 9.0 and 11.0). The *arrowheads* with *solid lines* indicate SOD1 subunits, and *arrowheads* with *broken lines* indicate modified SOD1 subunits.

fractions were then subjected to reducing SDS-PAGE and Western blotting. Since incubation with 5 mM H_2O_2 caused oxidation of almost all histidine and cysteine residues in bovine SOD1 (3), it is thought that negatively charged molecules were generated in both SOD1s. As shown in the *upper panels* of Fig. 2, *A* and *B*, several peaks containing oxidized SOD1 proteins were eluted with similar patterns in both SOD1s. However, the results of Western blotting were quite different (*lower panels* in Fig. 2, *A* and *B*). In oxidized 2-ME-SOD1, only one fragment (labeled with an *asterisk*) from the first peak and slight polymer bands from the last fractions, which were obtained by washing the column with 0.5 M KCl, were observed (Fig. 2*A*). The single fragment resulting from oxidation of 2-ME-SOD1 has been identified by Ookawara *et al.* (5) as a large fragment cleaved between Pro^{62} and His^{63}. Because Ookawara *et al.* (5) also used recombinant human SOD1 (2-ME-SOD1) obtained from Ube Industries Ltd., it can be concluded that the identity of the single fragment in the present study and that of Ookawara *et al.* (5)

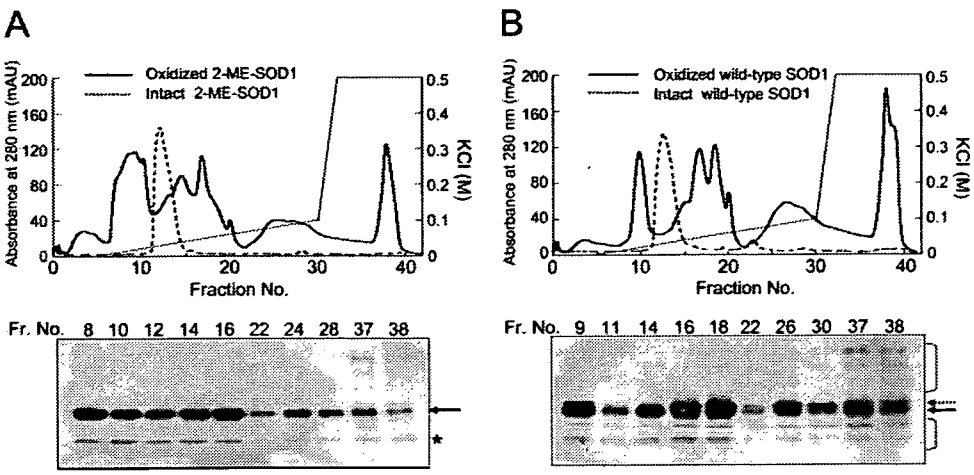

FIGURE 2. **Separation of oxidized SOD1s with a MonoQ column.** 2-ME-SOD1 and wild-type SOD1 were incubated with 5 mM H_2O_2 for 1 h and were applied to a MonoQ column; some fractions were subjected to reducing SDS-PAGE and Western blot analyses. *A*, chromatogram profiles of oxidized and intact 2-ME-SOD1 separated with MonoQ column (*top*), and Western blot analysis of some fractions indicated (*bottom*). *B*, chromatogram profiles of oxidized and intact wild-type SOD1 separated with MonoQ column (*top*), and Western blot analysis of some fractions indicated (*bottom*). SOD1 proteins in *A* and *B* were immunostained with anti-SOD1. The *arrowheads* with *solid lines* indicate SOD1 subunits, and *arrowheads* with *broken lines* indicate modified SOD1 subunits. *mAU*, milliabsorbance units.

are the same. In contrast, oxidation of the wild-type SOD1 resulted in not only the upper band but also in several additional fragments and polymer bands (Fig. 2*B*). Oxidation of Cys^{111} may become a trigger of fragmentation and polymerization. Zhang *et al.* (8) reported that a covalently cross-linked dimer (polymer) of human SOD1 was induced by bicarbonate and H_2O_2. Therefore, the effects of bicarbonate on the oxidation of 2-ME-SOD1 and wild-type SOD1 were investigated. However, no difference in dimer formation between the two SOD1 variants was observed (data not shown), suggesting that the cross-linkage between monomers was not mediated by Cys^{111}.

Identification of the Molecule in the Upper Band—Next, the identity of the molecule in the upper band was explored. Slow stirring in miliQ water did not cause fragmentation and polymerization of SOD1 but generated the upper band. Thus, in order to exclude effects of the buffer system, 2-ME-SOD1 and wild-type SOD1 were oxidized by stirring in miliQ water. Then the molecular masses were measured by MALDI-TOF MS. The air-oxidized wild-type SOD1 showed two masses, 15,792 and 15,838 *m/z*, but the mass of 2-ME-SOD1 did not change (Fig. 3*A*). Fig. 3*B* shows the elusion patterns of air-oxidized 2-ME-SOD1 and wild-type SOD1 on the MonoQ column. The stirred wild-type SOD1 (*solid line*) was separated into two peaks (*a* and *b*), whereas the stirred 2-ME-SOD1 (*dotted line*) was not separated. MALDI-TOF MS also showed that the SOD1 protein in peak *b* also gave two masses, 15,793 and 15,841 *m/z* (Fig. 3*C*), and gave two bands on reducing SDS-PAGE (Fig. 3*D*). It is noteworthy that the SOD activity in peak *b* (3716 units/mg) was similar to the activity in peak *a* (3753 units/mg) and that SOD1 proteins in both peaks retained more than 90% of SOD activity compared with the original wild-type SOD1. These results suggested that oxidative modification at Cys^{111} did not affect on SOD activity and that His residues in the active site were still intact. The difference in mass units between the SOD1 subunit in the upper band and the SOD1 subunit in the original band appeared to be about 48, suggesting the presence of three oxygens at Cys^{111}. Next, the upper and original bands from reducing SDS-PAGE (Fig. 3*D*) of peak *b* from the MonoQ column were clipped out, alkylated with IA, and digested with trypsin. The resultant peptides were subjected to MALDI-TOF MS analyses. In the *upper band*, a major mass, 2505 *m/z*, corresponding to tryptic peptide 92–115 (2457 *m/z*) plus 48 was detected. A minor mass, 2489 *m/z*, corresponding to tryptic peptide 92–115 plus 32 was also observed (Fig. 3*E*). In contrast, in the original band, a mass of 2514 *m/z* resulting from carbamidemethylation (plus 58) of tryptic peptide 92–115 was detected (Fig. 3*F*). These results indicate that amino acids in residues 92–115, probably Cys^{111}, in the upper band, were oxidized with two or three molecules of oxygen (Cys^{111}-SO_2H or Cys^{111}-SO_3H). However, the amounts of these peptides were too small for MS/MS analyses to determine the amino acid sequence.

To obtain greater quantities of oxidized peptides, SOD1 proteins in peaks *a* and *b* separated with the MonoQ column (Fig. 3*B*) were reduced by DTT, alkylated with IA, and digested with lysylendopeptidase, but not with trypsin. The resultant peptides were applied to a reverse-phase high performance liquid chromatograph (ODS column). As shown in Fig. 4*A*, the HPLC elution profiles were nearly identical, but two additional peaks (*d* and *e*) were observed after the last peak (*c*) only in digests from peak *b* of the MonoQ column (*i.e.* the *lower panel*). Peak *c* has already been identified as residues 92–122 containing carbamidemethylated Cys^{111} in previous work (25). When fractions containing the additional peaks *d* and *e* were reapplied to the ODS column, four fractions containing three distinct peaks were obtained (Fig. 4*B*). Each fraction was subjected to MALDI-TOF MS analyses. As a result, peptide *c* in fractions 1 and 2 corresponded to residues 92–122 containing carbamidemethylated Cys^{111} (3320.5 *m/z*), as expected. Peptide *d*, in fractions 2 and 3, and peptide *e*, in fractions 3 and 4, gave masses corresponding to residues 92–122 plus 32 (3295.5 *m/z*) and residues 92–122 plus 48 (3311.6 *m/z*), respectively (Fig. 4*C*).

To directly demonstrate the formation of Cys^{111}-SO_2H and Cys^{111}-SO_3H, these peptides (*c*–*e*), were further analyzed by infusion ESI MS/MS. This method was used to ascertain the site of oxidative modification of SOD1 by determination of the amino acid sequence of the peptides. The amino acid sequence of the peptide 92–122 was determined based on the assumption that Cys^{111} was modified with carbamidemethyl (Fig. 5*B*), sulfinic acid (SO_2H) (Fig. 5*C*), and sulfonic acid (SO_3H) (Fig. 5*D*), respectively. The mass of peptide *c* (3320.5 *m/z*), Cys-carbamidemethyl ($[M + 2H]^{2+}$ = 1661.2 *m/z*) gave the major fragment ions, y5 (611.3 *m/z*), y10 (1152.0 *m/z*), y12 (1424.6 *m/z*), y13 (1561.7 *m/z*), and y21* ($[M + 2H]^{2+}$ = 1161.0 *m/z*), indi-

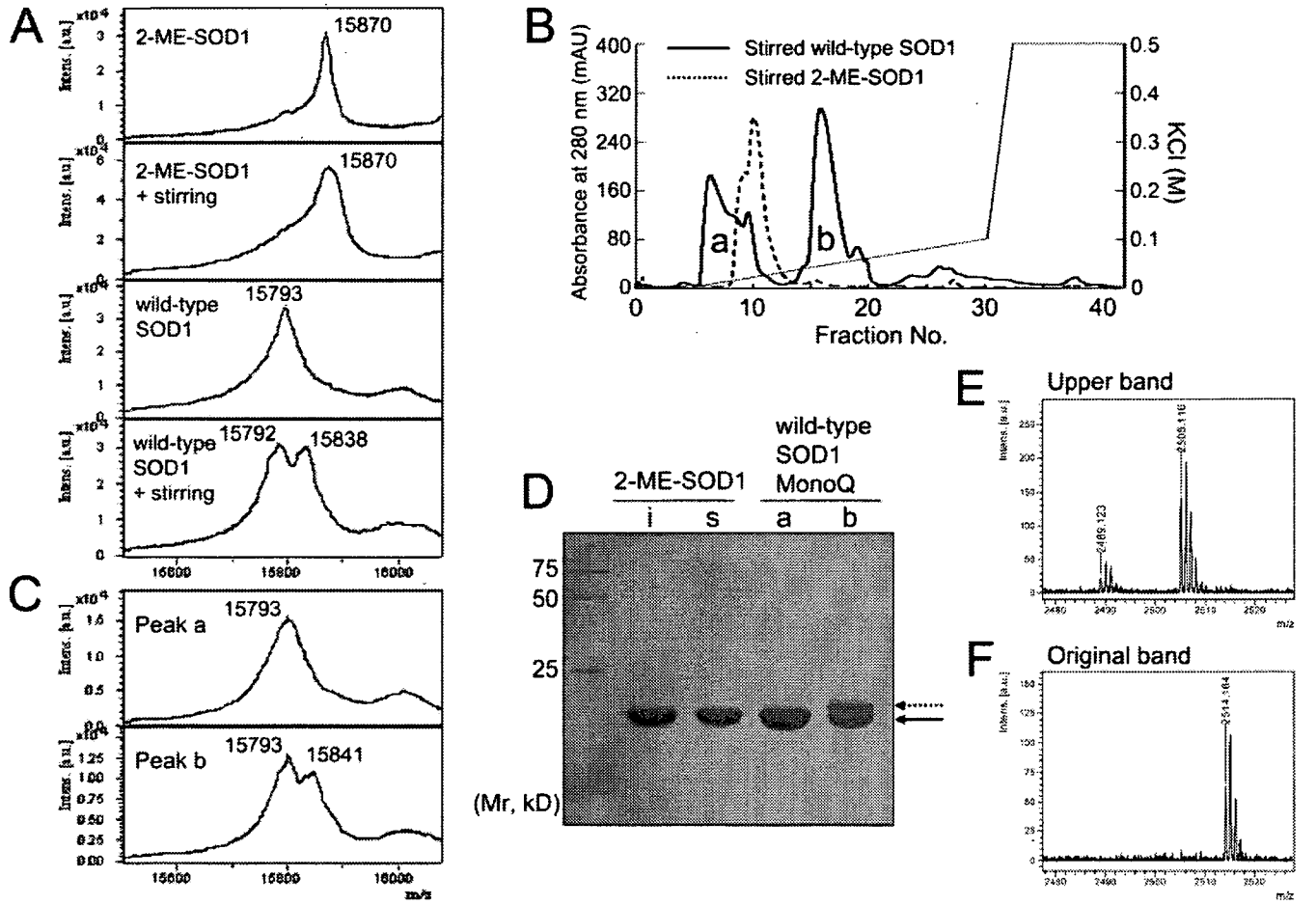

FIGURE 3. **Analyses of upper and original bands on SDS-PAGE.** *A*, MALDI-TOF MS spectra of intact and stirred 2-ME-SOD1 and wild-type SOD1, respectively. *B*, chromatogram profiles of stirred wild-type SOD1 and 2-ME-SOD1 on a MonoQ column. *C*, MALDI-TOF MS spectra of SOD1 in peaks *a* and *b*, separated with a MonoQ column (*B*). *D*, SDS-PAGE of intact (*i*) and stirred (*s*) 2-ME-SOD1 and SOD1s in peaks *a* and *b*. The *arrowheads* with *solid lines* indicate SOD1 subunits, and *arrowheads* with *broken lines* indicate modified SOD1 subunits. Precision Plus protein standards purchased from Bio Rad were used for the molecular weight marker (*left side*). *E* and *F*, MALDI-TOF MS spectra of tryptic peptides (residues Asp^{92}–Arg^{115}) from the upper band (*E*) and the original band (*F*), respectively, in the *right lane* of *D*. *mAU*, milliabsorbance units.

cating that Cys^{111} was carbamidemethylated, as expected (Fig. 5*E*). The mass of peptide *d* (3295.5 *m/z*) ([M + 2H]$^{2+}$ = 1648.3 *m/z*) gave the major fragment ions, y11 (1264.6, *m/z*), y12 (1399.7 *m/z*), y13 (1536.7 *m/z*), and b20 (2031.6 *m/z*), which was identified to be residues 92–122 containing Cys^{111}-SO_2H (Fig. 5*F*). Furthermore, the mass of peptide *e* (3311.6 *m/z*) ([M + 2H]$^{2+}$ = 1657.2 *m/z*) gave the major fragment ions, y9 (1038.6 *m/z*), y12 (1415.6 m/z), y13 (1552.7 *m/z*), y18 (2012.0 m/z), and y21 (2310.8 *m/z*), indicating that Cys^{111} was oxidized to Cys-SO_3H (Fig. 5*G*). Analyses based on the assumption that His^{110} and/or His^{120} were oxidized to 2-oxo-histidine showed that the corresponding y ions and b ions were absent (data not shown). These results clearly indicated that Cys^{111} was readily oxidized to Cys-SO_2H, which underwent further oxidation to Cys-SO_3H without His oxidation by air, and that the peroxidation of SOD1 at Cys^{111} resulted in the upper band shift in reducing SDS-PAGE.

Anti-C111ox-SOD1 Recognized Only Cys^{111}-peroxidized SOD1—To explore the possibility of immunological detection of Cys^{111}-peroxidized SOD1 (Cys^{111}-SO_3H-SOD1), a rabbit polyclonal antibody against the peptide containing Cys^{111}-SO_3H was prepared. The antiserum was purified to exclude the reactivity with reduced form SOD1 (Cys^{111}-SH) by affinity columns as described under "Experimental Procedures." The resultant IgG, which was denoted as anti-C111ox-SOD1, reacted with only the upper band of Cys^{111}-peroxidized SOD1 but neither the original band of wild-type SOD1 nor 2-ME-SOD1 (Fig. 6*A*). These data further demonstrated that the upper band is the oxidized form of SOD1 containing sulfonylated Cys^{111}. Also, in ELISA experiments, the anti-C111ox-SOD1 specifically reacted with IA-treated air-oxidized wild-type SOD1, but neither with 2-ME-SOD1 nor with IA-treated wild-type SOD1 (Fig. 6*B*). However, when wild-type SOD1 was not treated with IA before ELISA, the wild-type SOD1 was also reacted with anti-C111ox-SOD1, indicating that SH of Cys^{111} of the wild-type SOD1 was oxidized during coating on the 96-well plate.

Two-dimensional Gel Electrophoresis Characterization of Oxidized SOD1—It is well known that human, bovine, and recombinant human SOD1 proteins have several charge isomers detected by HPLC, isoelectric gel focusing, or two-dimensional gel electrophoresis (26, 30, 31). The reason for the heterogeneity is still unknown, although some hypotheses, such as different metallation, different conformation, and different oxidation of Cys residues, were presented (13, 26). Thus, two-dimensional gel electrophoresis of oxidized SOD1 was performed